SCIEPublish

*Review*

# Research Progress on High-Entropy Fibrous Materials

**Yulong Wang [1], Xue Shen [1], Tengyu Du [1], Zeyu Wang [1], Zhigang Yang [1,*], Gang Yu [1], Guoqiang Qin [1], Shengya He [2,*], Zhi Wang [1] and Lei Wen [3]**

[1] School of Materials Science and Engineering, Engineering Research Center of Matamaterials and Microdevices, Shijiazhuang Tiedao University, Shijiazhuang 050043, China; 1171755512@qq.com (Y.W.); 3300304797@qq.com (X.S.); 1819354811@qq.com (T.D.); 584907350@qq.com (Z.W.); 819069099@qq.com (G.Y.); 57906085@qq.com (G.Q.); 282715455@qq.com (Z.W.)

[2] GRINM (Guangdong) Institute for Advanced Materials and Technology, Foshan 528051, China

[3] Mechanics Engineering Department, Shijiazhuang Tiedao University, Shijiazhuang 050043, China; WL0921@126.com (L.W.)

* Corresponding author. E-mail: yangzhigang@stdu.edu.cn (Z.Y.); heshengya@grinm.com (S.H.)

Received: 30 April 2025; Accepted: 11 June 2025; Available online: 19 June 2025

**ABSTRACT:** Due to their lightweight, high strength, and thermal resistance, HEFMs exhibited significant potential in aerospace, energy storage, environmental protection, and defense. This review systematically presented the research progress on high-entropy fibrous materials (HEFMs), covering their fundamental concepts, fabrication methods, crystal structure characteristics, performance advantages, and application fields. The different crystal structure types and fabrication techniques of high-entropy ceramic fibers and high-entropy alloy fibers were discussed. Additionally, the mechanical property advantages of HEFMs and their applications in thermal insulation materials, catalysis, and energy storage were analyzed. Finally, the current challenges in HEFM research and provide an outlook on future development directions.

**Keywords:** High-entropy fibrous materials (HEFMs); Crystal structure; Fabrication techniques; Applications; Challenges

© 2025 The authors. This is an open access article under the Creative Commons Attribution 4.0 International License (https://creativecommons.org/licenses/by/4.0/).

## 1. Introduction

High-entropy materials (HEMs) are typically defined as alloys or compounds composed of five or more principal elements, each with a molar fraction generally ranging from 5% to 35%, resulting in a near-equiatomic configuration. This compositional design leads to a high configurational entropy (commonly exceeding 1.5 R) which thermodynamically favors the formation of stable single-phase solid solution structures over conventional multiphase mixtures or intermetallic compounds. In the advancement of modern materials science, High-Entropy Materials (HEMs) have emerged as a novel class of materials that have garnered significant attention due to their unique structural characteristics and exceptional properties [1–3]. The concept of HEMs was first introduced by Yeh et al. in 2004 and has since evolved into a pivotal research direction in the field of materials science. Unlike conventional alloys [4], which are typically composed of a primary element with minor additions of alloying elements to optimize performance, HEMs are generally composed of five or more principal elements in near-equiatomic ratios. The high degree of compositional mixing leads to the formation of highly disordered solid solution phases, fundamentally altering the material's microstructure and crystalline characteristics [5–8]. As a result, HEMs exhibit an expanded performance space and outstanding multifunctional properties in mechanical, thermal, electrical, and chemical aspects, making them highly promising for a wide range of applications.

In the early stages of high-entropy materials (HEMs) research, the focus is primarily on metallic alloys, particularly High-Entropy Alloys (HEAs). Compared to conventional single-principal-element fibers or traditional alloy-based fibers, HEA-based fibrous materials exhibit greater phase stability, slower diffusion kinetics, and uniform element distribution, which exhibit exceptional strength, hardness, and corrosion resistance [4,9–12]. However, in recent years, researchers have progressively extended the high-entropy concept to various material systems, including ceramics, coatings, composites, and polymers [13–15]. Among them, High-Entropy Fibrous Materials (HEFMs) have attracted

https://doi.org/10.70322/htm.2025.10014

increasing attention due to their lightweight nature, structural stability, high strength, and thermal resistance [16–18]. These unique properties endow HEFMs with promising applications in aerospace, energy storage, catalysis, and thermal insulation, highlighting their potential as advanced structural and functional materials in diverse technological fields.

As shown in Figure 1, fibrous materials are widely utilized in structural reinforcement, functional composites, and intelligent materials [3,19–24]. Traditional fibrous materials primarily rely on the optimization of a single or a limited number of components, such as ceramic and metallic fibers, whose performance is inherently constrained by their intrinsic physicochemical properties. In contrast, High-Entropy Fibrous Materials (HEFMs) have a homogeneous distribution of multiple components, resulting in unique microstructures and multi-scale interfacial effects [3,5,9,10,25–27]. These characteristics endow HEFMs with key high-entropy effects, including the Entropy Effect, Sluggish Diffusion Effect, Severe Lattice Distortion Effect, and Cocktail Effect [26]. These effects collectively contribute to enhanced mechanical, thermal, and chemical properties, significantly broadening the application potential of HEFMs in advanced materials engineering.

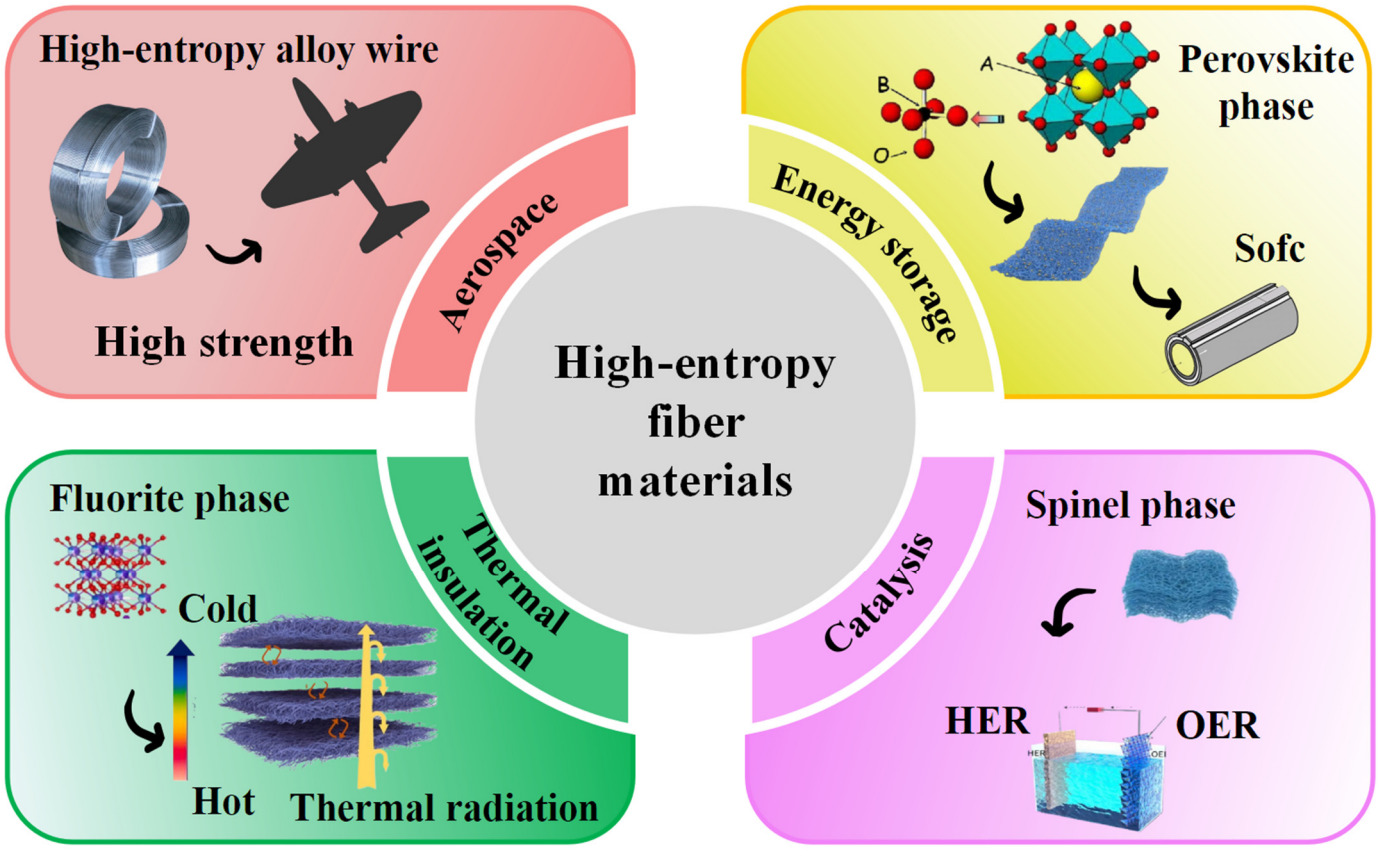


**Figure 1.** Initial Applications of High-Entropy Materials.

The research on High-Entropy Fibrous Materials (HEFMs) encompasses not only their synthesis methods, such as electrospinning, hot forging and drawing, cryogenic rolling, and glass-cladding techniques, but also their microstructural characterization and performance optimization. For instance, electrospinning enables the fabrication of high-entropy oxide nanofibers with precise nanoscale control, thereby enhancing their mechanical and functional properties [28–33]. Additionally, hot forging and drawing techniques utilize high-temperature plastic deformation and multi-directional compression to refine grain structures [34], optimize texture, improve fiber strength and ductility, and reduce defect sensitivity. This process could enhance the mechanical properties, fatigue resistance, and manufacturability of high-entropy alloy fibers.

Compared to conventional fibrous materials, HEFMs exhibit outstanding multi-functional properties. In terms of mechanical performance, the synergistic effect of multiple components leads to complex crystal structures and enhanced phase [35] stability, resulting in higher tensile strength and fracture toughness. Moreover, the high surface area and nanoscale effects of HEFMs provide unique advantages in thermal, optical, and electrical properties. For example, high-entropy ceramic fibers demonstrate remarkable oxidation resistance and thermal stability even in extremely high-temperature environments, making them ideal candidates for high-temperature structural applications [28,36].

Despite significant theoretical and HEFMs, they still face several challenges. First, the precise design of multi-component systems and microstructural control is critical to ensuring material stability and consistency, which remains a major research focus. Second, the synthesis of high-entropy materials often involves complex fabrication processes, making it imperative to enhance process controllability and scalability for large-scale production. Third, due to the multi-component nature of high-entropy materials, the underlying interaction mechanisms among different elements are not yet fully elucidated. Further studies are required to investigate their formation mechanisms, crystal structures, and the evolution of multi-scale properties. The exceptional properties of HEFMs largely stem from their unique crystalline structure. Unlike traditional fibrous materials, HEFMs exhibit a random distribution of multiple elements, leading to significant lattice distortion effects and long-range order–short-range disorder characteristics at the atomic scale [37]. A deeper understanding of the crystalline structure, phase stability, phase transformation behavior, and defect evolution mechanisms of HEFMs is essential for further performance optimization and broaden of their application spectrum.

The following discussion will focus on the distinct crystalline structural characteristics of two types of high-entropy fibrous materials, exploring their formation mechanisms and potential applications. Additionally, we will examine the primary fabrication methods for these two high-entropy fibrous materials alongside the challenges faced in their development and future research directions. This analysis aims to provide a scientific foundation for the advancement and optimization of high-entropy fibrous materials, offering insights for their future research and technological application.

## 2. High-Entropy Fibrous Materials

High-entropy fibrous materials can be broadly categorized into high-entropy ceramic fibers and high-entropy alloy fibers. As shown in Figure 2, each exhibits outstanding performance in distinct application fields. High-entropy ceramic fibers demonstrate exceptional high-temperature resistance, catalytic activity, and electrochemical energy storage capabilities, making them highly suitable for extreme environments and functional applications [29,36,38].

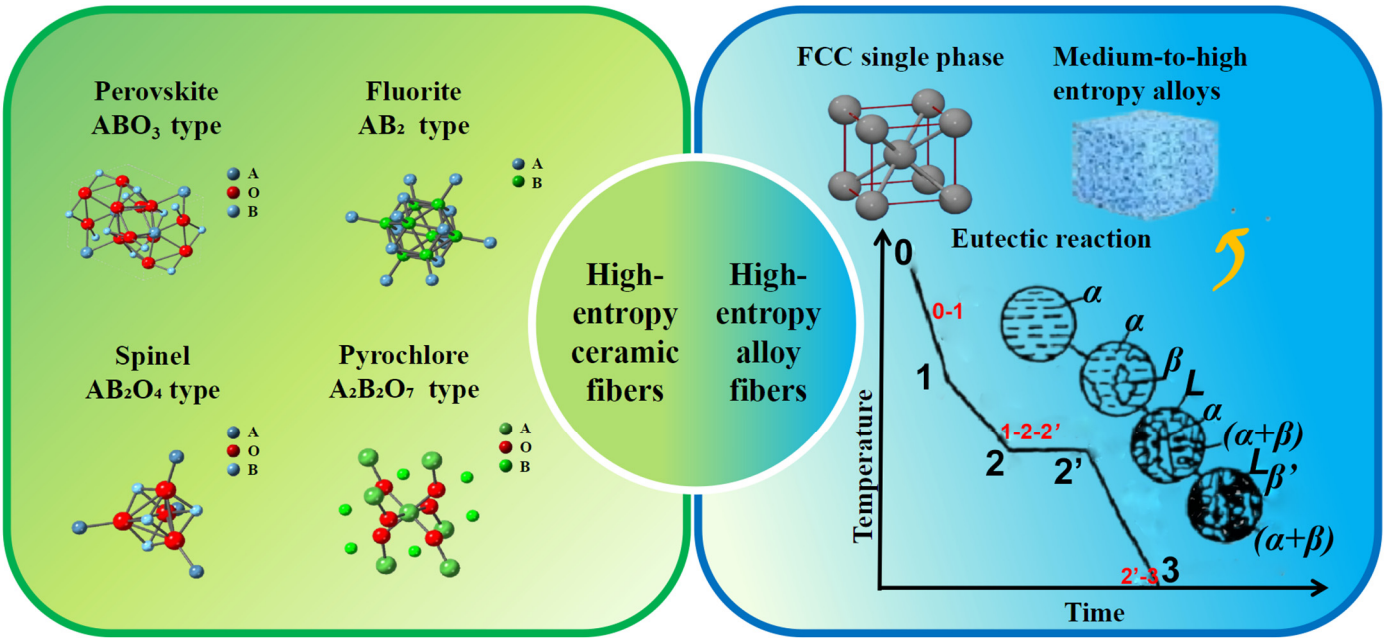


**Figure 2.** Main Classifications of High-Entropy Fibers.

### *2.1. High-Entropy Ceramic Fibers*

This section provides an overview of the different structural types of high-entropy ceramic fibers (HECFs), including fluorite-type, perovskite-type, spinel-type, and pyrochlore-type structures [39,40]. Furthermore, it explores their applications in high-temperature thermal insulation, solid electrolytes, electrochemical catalysis, and energy storage, highlighting their potential in advanced functional materials for extreme environments and next-generation technologies.

#### 2.1.1. Fluorite-Type Structure ($AB_2$-Type)

In the fluorite-type structure, cations (such as certain metal cations in high-entropy oxides) form a face-centered cubic (FCC) structure, while anions (such as oxygen ions) occupy all the tetrahedral interstitial sites within the cubic

unit cell [41–43]. Each cation is coordinated by eight anions, whereas each anion is surrounded by four cations. The fluorite-type structure is one of the high-entropy crystal structures in ceramics. Currently, the predominant method for fabricating high-entropy oxide ceramics is the solid-state sintering method [44–47], which involves the stoichiometric mixing of multiple metal oxide powders, followed by high-temperature sintering to achieve phase homogenization. Solid-state sintering typically requires elevated temperatures and prolonged sintering durations to facilitate diffusion and phase formation.

A novel approach involves using viscose fibers as a template and vacuum-impregnating them in a mixed metal nitrate solution. After undergoing water washing, centrifugation, drying, and thermal treatment, it is possible to successfully obtained high-entropy oxide ceramic fibers (as shown in Figure 3). The resulting fibers, such as $(Ce_{0.2}Zr_{0.2}Hf_{0.2}Sn_{0.2}Ti_{0.2})O_2$, exhibited a uniform morphology and a single-phase fluorite structure [48]. This method offers several advantages, including precise stoichiometric control, excellent dispersion of metal ions, low energy consumption, mild reaction conditions, and environmental sustainability.

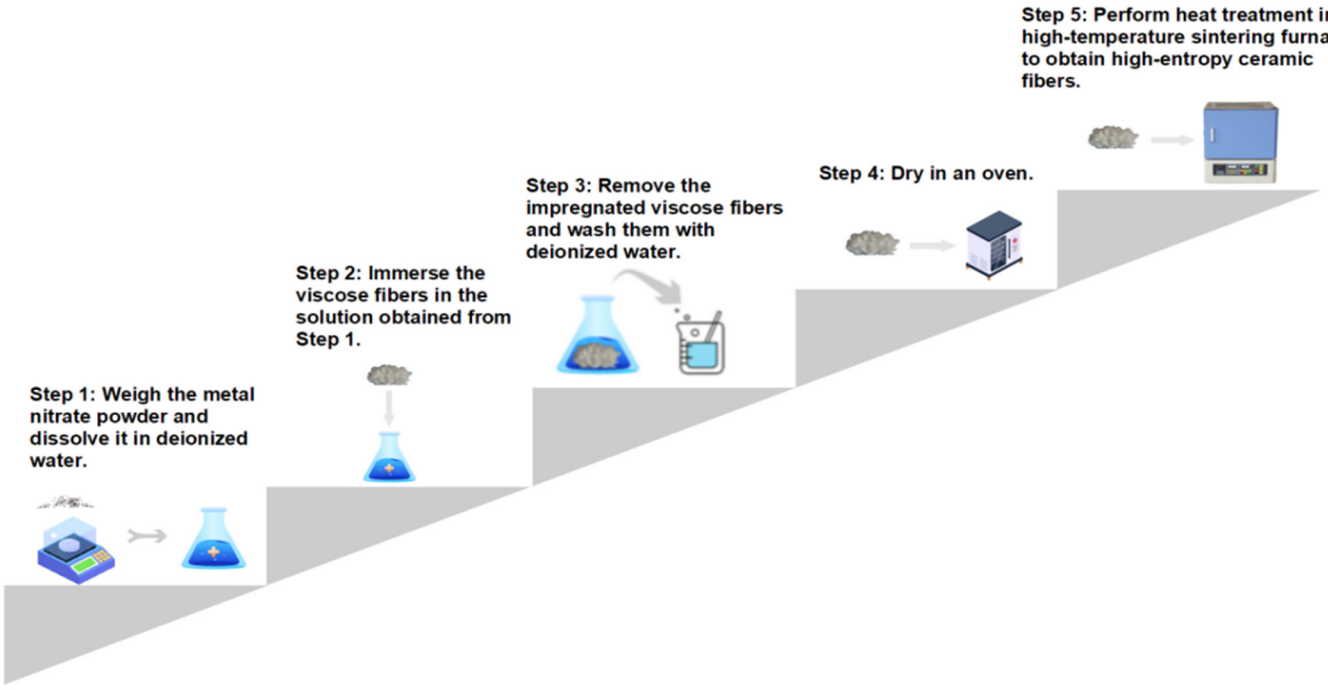


**Figure 3.** High-entropy ceramic fibers fabricated using viscose fibers as a template.

Researchers [49–51] have discovered that the fluorite-phase structure exhibits excellent ionic conductivity. This is attributed to the relatively open anionic conduction channels within its structure, which facilitate ion migration under an electric field. As a result, this material has already been applied in fields such as solid electrolytes prior to being processed into fibrous morphologies [52,53].

For instance, researchers [54] have developed a high-entropy oxide ceramic material using a simple and low-cost fabrication method. This material demonstrates excellent electrical conductivity and high-temperature stability, making it suitable as an electrolyte for high-performance ion batteries. Furthermore, another study explored the application of high-entropy oxides in lithium-ion batteries [55], where one-dimensional $CoZnCuNiFeZrCeO_x$-PMA nanofibers were fabricated via an electrospinning process (as shown in Figure 4a,b, exhibiting outstanding electrochemical performance. The findings suggest that fluorite-phase high-entropy materials hold significant potential for the fabrication of electrolyte fibers in ion batteries.

Fluorite-type high-entropy oxide ceramics exhibit excellent thermal stability and low thermal conductivity, making them suitable for high-temperature thermal insulation materials. Liu Yufu and colleagues from Southeast University synthesized a high-entropy oxide, $Hf_{(0.15–0.3)}Zr_{(0.15–0.3)}Ce_{(0.15–0.3)}Y_{(0.05–0.3)}Al_{(0.05–0.3)}O_{2–\delta}$, using the sol-gel method [50]. This oxide features stable Al–O bonds, high-temperature stability, good powder homogeneity, and a high specific surface area, enabling its application as a high-performance thermal barrier coating.

However, compared to coating materials, high-entropy fiber materials exhibit superior mechanical properties, longer service life, enhanced high-temperature stability, and improved oxidation resistance. Additionally, they offer

advantages in adaptability and environmental sustainability. Therefore, high-entropy ceramic fibers with a fluorite-type structure also hold significant potential for applications in high-temperature thermal insulation.

In addition to its applications in solid electrolytes and related fields, high-entropy ceramic fibers with this structure exhibit exceptional mechanical properties, particularly in terms of durability and stability under extreme temperatures [26,28,38]. The fibrous morphology enhances the material's strength and flexibility through processing, making it more durable in practical applications and suitable for long-term use at high temperatures.

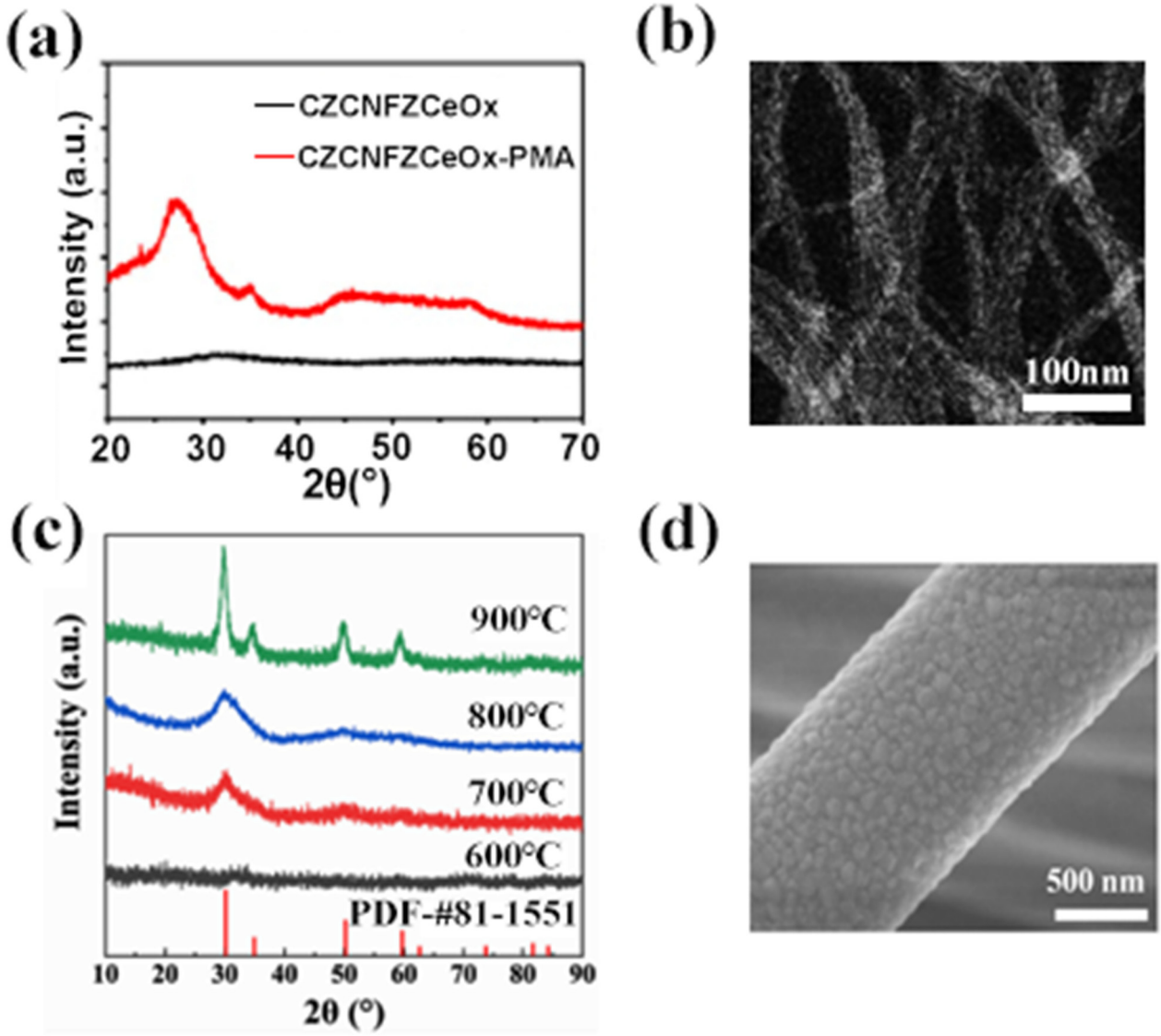


**Figure 4.** (**a**) XRD patterns of CoZnCuNiFeZrCeOx and CoZnCuNiFeZrCeOx-PMA SNWs. (**b**) HAADF−STEM image of CoZnCuNiFeZrCeOx-PMA SNWs [55]. (**c**) XRD of the ZHTGY fibers hold at different heat treatment temperature for 2 h. (**d**) SEM of the fibers hold at 1000 °C for 2 h [56].

Deng et al. [56] successfully synthesized $(Zr_{0.2}Hf_{0.2}Ti_{0.2}Gd_{0.2}Y_{0.2})O_{2-\delta}$ (ZHTGY) high-entropy oxide fibers through molecular design (as shown in Figure 4c,d). Compared with other high-entropy oxide materials, ZHTGY fibers exhibit a lower crystallization temperature and outstanding high-temperature stability. No phase transition is observed over a wide temperature range from room temperature to 1500 °C, demonstrating their excellent thermal reliability. Furthermore, the ZHTGY fiber membranes exhibit low density and high tensile strength, offering excellent flexibility. They can be freely bent even in extreme environments such as butane flames or liquid nitrogen, demonstrating remarkable mechanical resilience. With ultralow density and high-temperature structural stability, these fiber membranes provide exceptional thermal insulation performance. This study introduces a novel approach for fabricating high-entropy oxide fibers, paving the way for the development of lightweight, high-temperature thermal protection materials.

### 2.1.2. Perovskite-Type Structure ($ABO_3$-Type)

The perovskite-type structure ($ABO_3$-type) is typically composed of a larger cation at the A-site and a smaller cation at the B-site, along with oxygen anions [57–59]. In this structure, A-site cations are located at the corners of the cubic unit cell, B-site cations occupy the body center, and oxygen anions reside at the face centers. In high-entropy oxide fibers, the A-site and B-site can be occupied by multiple metal cations, forming a high-entropy perovskite structure. The synthesis of perovskite-type high-entropy oxide ceramics is often achieved through solid-state sintering methods [11,47,57,60,61]. Zhang et al. [62] successfully synthesized A-site equimolar perovskite-type high-entropy oxide ceramics $(La_{0.2}Li_{0.2}Ba_{0.2}Sr_{0.2}Ca_{0.2})TiO_3$ via the solid-state sintering method and investigated the effects of sintering temperature on the phase structure and electrical properties of high-entropy ceramics.

Perovskite-type high-entropy oxide ceramics exhibit excellent properties, making them highly promising for applications in electronic information technology, battery materials, and electrochemical catalysis. In the field of electronic information field, with the rapid advancement of modern communication technologies, microwave dielectric ceramics have garnered significant attention due to their widespread applications in mobile communications, electronic devices, and military radar systems. Ma et al. [63] successfully synthesized a high-entropy perovskite-structured microwave dielectric ceramic, which exhibits excellent dielectric properties, including a high dielectric constant. This study provides valuable insights for designing high-entropy perovskite microwave dielectric ceramics with superior dielectric performance.

In the battery materials field, the research team led by Associate Professor Zhang Ze [64] fabricated high-entropy perovskite oxide $La_{0.8}Sr_{0.2}(Cr_{0.2}Mn_{0.2}Fe_{0.2}Co_{0.2}Ni_{0.2})O_3$ nanofibers using an electrospinning process combined with calcination (as shown in Figure 5a,b). These nanofibers were employed as bidirectional electrocatalysts for the liquid-solid conversion process in lithium-sulfur batteries. The fibers effectively modulate the binding strength of soluble polysulfides, leading to high areal capacity and excellent cycling stability.

Additionally, Fu et al. [65] developed a novel A-site high-entropy perovskite oxide $La_{1/6}Pr_{1/6}Nd_{1/6}Ba_{1/6}Sr_{1/6}Ca_{1/6}FeO_{3-\delta}$ (LPNBSCF) nanofiber cathode via electrospinning for application as a mid-temperature cobalt-free cathode in solid oxide fuel cells (SOFCs) (as shown in Figure 5c,d). This material demonstrated good compatibility with electrolytes, and the tested power density exceeded that of cells using $La_{0.6}Sr_{0.4}FeO_{3-\delta}$ (LSF) nanofiber cathodes, confirming the great potential of LPNBSCF nanofibers for SOFC applications.

Currently, research on the application of perovskite-type high-entropy oxide ceramics in electrochemical catalysis is mainly confined to the preparation of solid powders. Liu et al. [66] synthesized $Ba_x(FeCoNiZrY)_{0.2}O_{3-\delta}$ high-entropy perovskite oxides via liquid-phase chelation, gelation, and calcination for use as electrocatalysts in nitrogen reduction reactions (NRR). That same year, the research team discovered that by modifying the nonstoichiometric ratio of A-site metal elements, the material exhibited a higher density of oxygen vacancies, thereby enhancing nitrogen reduction activity.

More recently, Zhu et al. [67] investigated cocktail effects in high-entropy perovskite oxide hollow nanofibers. Specifically, they examined $La_{0.5}Sr_{0.5}Mn_{0.15}Fe_{0.15}Co_{0.4}Ni_{0.15}Cu_{0.15}O_3$ nanofibers (as shown in Figure 5e,f), which demonstrated exceptional oxygen evolution reaction (OER) activity under alkaline conditions. Their findings provide guidance for rationally utilizing the cocktail effect in multi-site electrocatalysts. Thus, future research on the fabrication of perovskite-type high-entropy ceramic fibers is expected to be a key focus area.

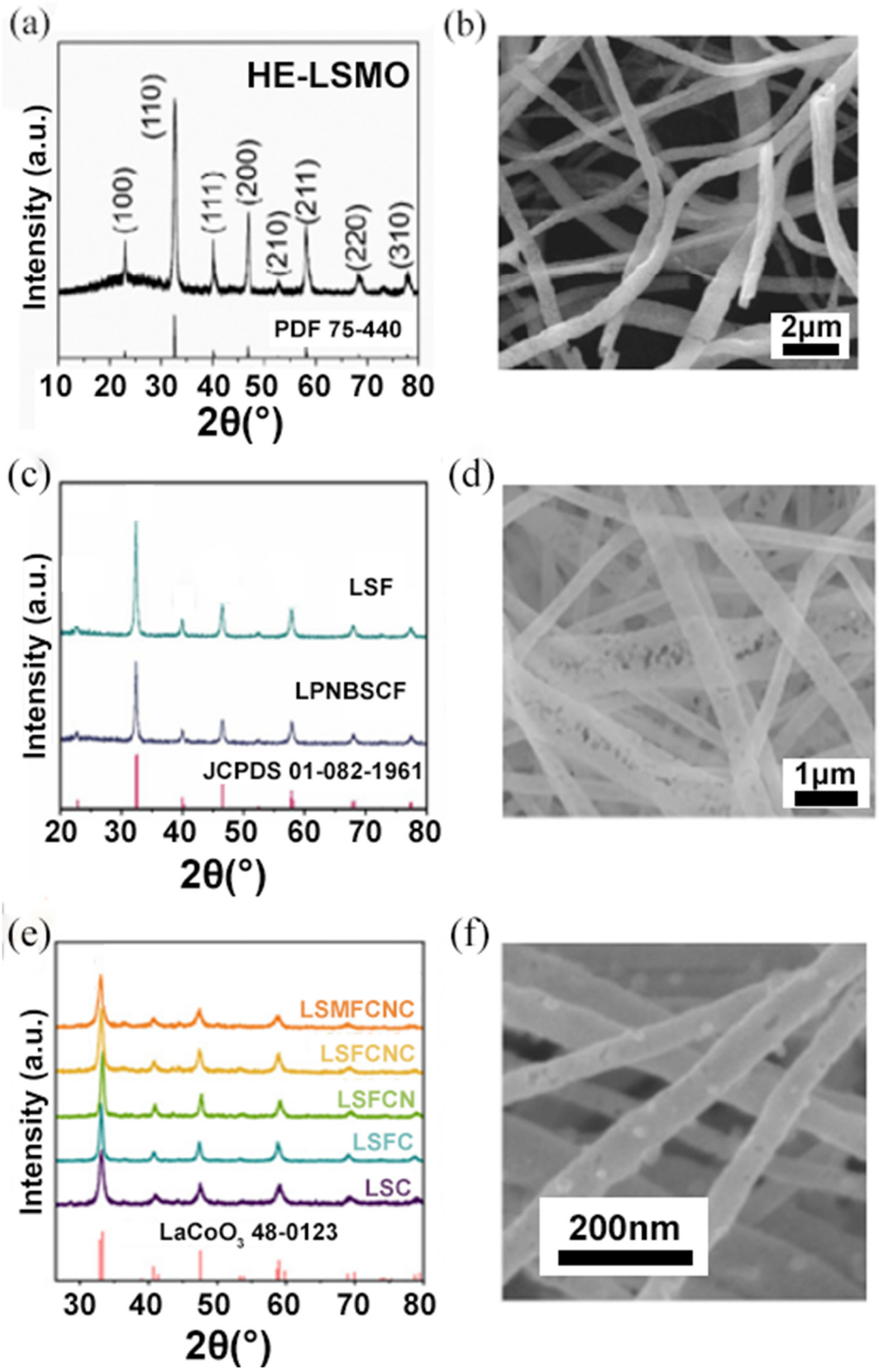


**Figure 5.** (**a**) XRD pattern, (**b**) SEM image [64], (**c**) XRD patterns of LSF and LPNBSCF nanofibers after calcining at 800 °C for 3 h in air, (**d**) magnified images of the LPNBSCF nanofibers after sintering [65], (**e**) XRD patterns of the as-prepared LSMFCNC and the corresponding Controls, (**f**) FE-SEM image of the LSMFCNC [67].

### 2.1.3. Spinel-Type Structure ($AB_2O_4$-Type)

In the spinel crystal structure, oxygen ions form a cubic close-packed (CCP) arrangement, where A-site cations occupy 1/8 of the tetrahedral interstices, and B-site cations occupy 1/2 of the octahedral interstices [68–72]. In high-

entropy spinel oxide fibers, both A-site and B-site can be occupied by multiple metal cations, forming a complex high-entropy structure.

Zhang et al. [73] developed a high-entropy spinel oxide nanofiber-based photocatalyst. This method involves dissolving equimolar metal salts in an organic solvent to form a stable solution, followed by electrospinning and high-temperature annealing to obtain one-dimensional high-entropy oxide nanofibers. The spinel-structured high-entropy oxide nanofiber photocatalyst produced by this method offers lower energy consumption and cost while achieving finer and more uniform nanofiber grains. Additionally, the structure can be effectively controlled by adjusting the calcination temperature.

High-entropy design enhances structural stability, electrochemical performance, and cycling life of materials through the synergistic effects of multiple principal elements [74]. Recent literature has reviewed the research progress on high-entropy spinel materials in lithium-ion batteries, with a focus on their design strategies and performance advantages when applied as cathodes, anodes, and solid-state electrolytes. The review also provides an outlook on the future prospects and challenges of these materials in next-generation energy storage devices, offering new insights for the development of high-safety, high-energy-density batteries.

High-entropy oxide fibers can serve as efficient electrocatalysts for the oxygen reduction (ORR) and hydrogen evolution reaction (HER), making them highly suitable for water electrolysis. Claudia et al. [68] synthesized three types of high-entropy oxide fibers for oxygen evolution reaction (OER) catalysis (as shown in Figure 6a,b), systematically studying the effects of calcination temperature on fiber morphology, spinel oxide crystallinity and inversion degree, oxygen vacancy concentration, and cation distribution within the lattice. Their results demonstrated that $(Cr_{1/5}Mn_{1/5}Fe_{1/5}Co_{1/5}Ni_{1/5})_3O_4$ nanofibers calcined at 500 °C exhibited the best electrocatalytic performance.

In the field of gas sensing, Li et al. [75] synthesized $(FeCoNiCrMn)_3O_4$ high-entropy oxides (HEOs) using a high-entropy alloy precursor. They investigated the crystal structure, microstructure, elemental valence states, and gas-sensing properties of this material. The sensor demonstrated a strong response to $NO_2$ at room temperature (RT), highlighting the potential application of $(FeCoNiCrMn)_3O_4$ in low-power gas sensors and expanding the range of materials available for RT gas sensors.

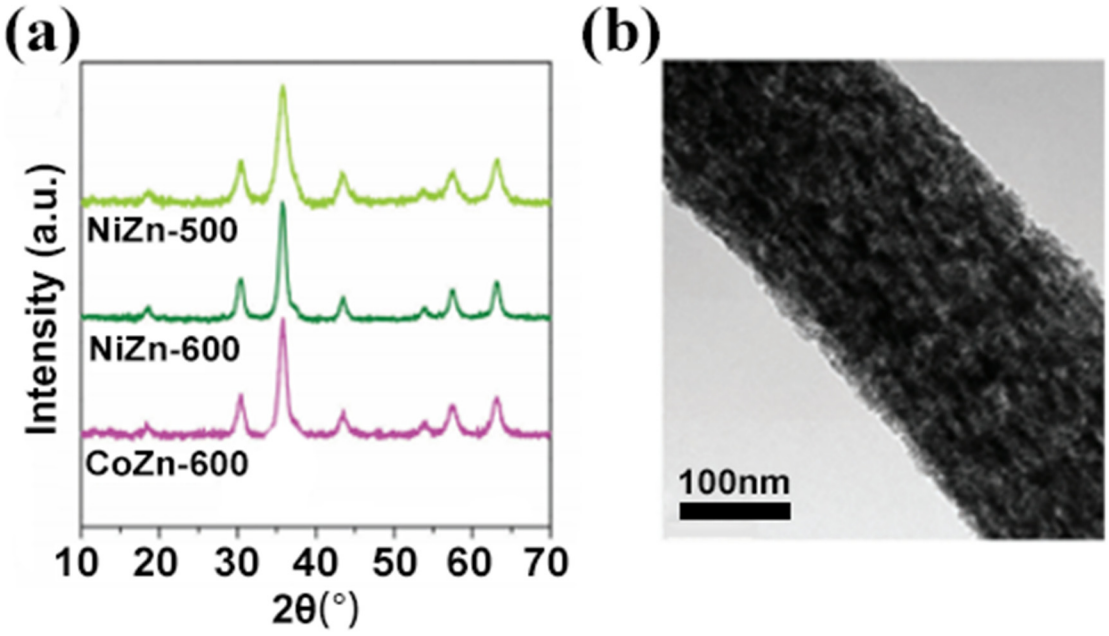


**Figure 6.** (**a**) XRD patterns, (**b**) TEM images of electrospun NFs [68].

### 2.1.4. Pyrochlore-Type Structure ($A_2B_2O_7$)

High-entropy pyrochlore ceramics, a class of high-entropy oxides composed of multiple metal elements, exhibit complex crystal structures. In this structure, oxygen ions form octahedral coordination units that are interconnected via corner-sharing, forming a three-dimensional framework [46,76–78]. The A-site cations are located within the voids of the octahedral framework, forming coordination bonds with surrounding oxygen ions, while the B-site cations reside at the center of the oxygen octahedra, forming stable chemical bonds with oxygen.

High-entropy pyrochlore materials are designed to enhance thermal stability, electrochemical performance, and mechanical properties through the incorporation of multiple elements, demonstrating great potential for applications in

high-temperature thermal insulation, battery materials, and electrocatalysis. Due to their structural diversity, high-entropy fiber materials can be engineered with tailored fiber morphologies, dimensions, and surface treatments to enhance their thermal insulation properties further. For instance, dispersed nanoparticles or porous structures can effectively suppress thermal conductivity, leading to more efficient thermal insulation.

Wang et al. [79] synthesized flexible high-entropy ceramic nanofiber membranes $(La_{0.2}Nd_{0.2}Sm_{0.2}Gd_{0.2}Yb_{0.2})_2Zr_2O_7$ (LNSGY) using electrospinning with a polyacrylate-based rare-earth zirconium precursor. (as shown in Figure 7a,b) Phase and microstructure analysis confirmed that LNSGY nanofiber membranes exhibited a dual-phase structure of defective fluorite and ordered pyrochlore. Upon thermal treatment, the grain size of LNSGY fibers increased, but their slow grain growth, excellent flexibility, and uniform fiber morphology contributed to low thermal conductivity at room temperature and high tensile strength and thermal stability at elevated temperatures. These properties indicate a strong potential for high-entropy ceramic nanofiber membranes in high-temperature insulation applications.

Due to their low density and high specific surface area, fiber materials are ideal for high-temperature insulation applications, such as in aerospace, aviation, and thermal protection systems for high-temperature industrial equipment. Their high-temperature stability and low thermal conductivity make them effective in preventing heat transfer under extreme conditions. With the rapid advancements in science and technology, new demands have emerged for high-temperature insulation materials, requiring them to be lightweight, thermally stable, and resistant to thermal shock and mechanical vibrations. These properties are essential for hypersonic vehicles, nuclear power generation, and chemical metallurgy, making them a critical class of next-generation high-temperature protection materials.

Zhao et al. [28] synthesized high-entropy ceramic nanofibers (HE-$RE_2Zr_2O_7$) using electrospinning, with a composition of $(La_{0.2}Sm_{0.2}Eu_{0.2}Gd_{0.2}Tm_{0.2})_2Zr_2O_7$. (as shown in Figure 7c,d) Phase and microstructural analysis confirmed the pure-phase structure with a uniform distribution of rare-earth elements. SEM images showed that the HE-$RE_2Zr_2O_7$ nanofibers maintained a dense structure after annealing at 1000 °C for 0–5 h. After annealing at 1000 °C for 0–2.5 h, the fiber diameter increased slightly, while the thermal conductivity remained low (0.23 $W \cdot m^{-1} \cdot K^{-1}$). The slow diffusion effect of high-entropy materials, coupled with the slow diameter growth and excellent thermal stability of HE-$RE_2Zr_2O_7$ fibers, further promotes their broad application as high-temperature thermal insulation materials.

In high-entropy pyrochlore structures, the presence of oxygen vacancies can modulate electrical and optical properties, which play a critical role in applications such as catalysis and energy storage. Although no specific studies have been reported on high-entropy pyrochlore oxide fibers, research on pyrochlore-type composite oxides has demonstrated their potential for diesel soot oxidation. Ai et al. [80] proposed the use of rare-earth pyrochlore $A_2B_2O_7$-type composite oxides to develop low-cost and highly efficient diesel soot combustion catalysts.

In solid-state battery applications for high-performance electric vehicles (EVs), the polymeric structure and chemical stability of high-entropy fibers makes them ideal building blocks for solid electrolytes, significantly enhancing battery energy density and cycle life [81]. Dou et al. [81] explored high-entropy-induced ceramic nanofibers with stable $Bi_2Ti_2O_7$-type pyrochlore phases as effective nanofillers to enhance the energy storage performance of polyetherimide (PEI) composites (as shown in Figure 7e,f). The linear pyrochlore phase, refined grain size, and increased amorphous content of high-entropy nanofillers resulted in significantly improved energy storage performance over a broad temperature range (25–150 °C). This breakthrough not only advances EV performance but also creates new opportunities for wider applications in electric transportation.

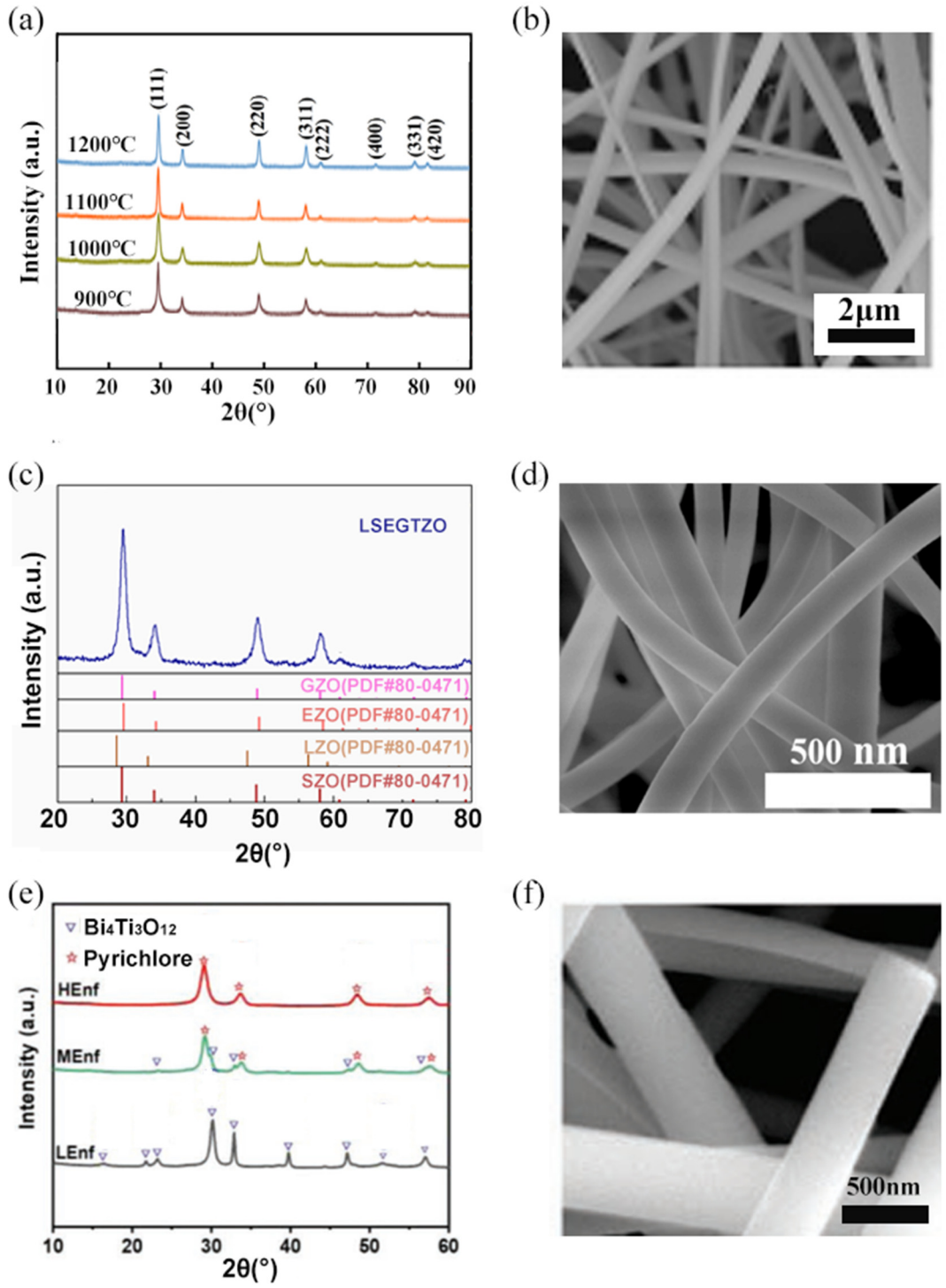


**Figure 7.** (**a**) XRD patterns of LNSGY nanofibrous membranes calcined at different temperatures, (**b**) SEM image of LNSGY nanofibrous membranes calcined at 1200 °C [79], (**c**) XRD patterns of the prepared HE-$RE_2Zr_2O_7$ fibers at 1000 °C with those of single component $Ln_2Zr_2O_7$ (Ln = La, Sm, Eu, Gd, Tm) obtained from ICDD/JCPDS cards, (**d**) SEM micrographs of HE-$RE_2Zr_2O_7$ fibers at 1000 °C [28], (**e**) XRD patterns of LEnf, MEnf, and HEnf, (**f**) SEM image of HEnF fiber [81].

### *2.2. High-Entropy Alloy (HEA) Fibers*

Currently, research on high-entropy alloy (HEA) fiber materials remains relatively limited. Compared to traditional bulk materials, HEA fibers are primarily focused on single-phase face-centered cubic (FCC) HEAs with good plasticity and eutectic HEAs [82].

HEA fibers (as shown in Figure 8) exhibit significant mechanical advantages over conventional bulk HEA materials. The fiber morphology enables grain refinement, leading to higher specific strength and stiffness while significantly enhancing fracture toughness, thereby preventing premature failure caused by grain boundary brittleness

in bulk materials [83]. Due to their small diameters and high aspect ratios, HEA fibers enable more uniform stress distribution, improving fatigue resistance and making them particularly effective in high-strain environments.

The nanoscale effects of HEA fibers further contribute to their superior deformation coordination under high temperatures or extreme loading conditions, reducing local stress concentrations and allowing the material to maintain high strength and ductility even at elevated temperatures [83]. The high-entropy effect enhances solid-solution strengthening and lattice distortion, optimizing the balance between mechanical performance and durability.

In contrast, bulk HEAs, due to their larger size, are more susceptible to microcrack propagation, leading to lower impact resistance and reduced fatigue life. Therefore, HEA fibers, with their superior strength, toughness, fatigue resistance, and high-temperature performance, hold great potential for applications in aerospace, wear-resistant protection, and flexible electronics.

Li et al. [84] successfully fabricated HEA fibers containing $Al_{0.3}CoCrFeNi$ using the thermal drawing method. The key innovation of this study lay in the application of the thermal drawing technique, where molten HEA material was stretched into fiber form, ensuring a uniform distribution of elements within the fibrous structure. This novel fabrication technique enhances the high-entropy effect within the alloy, significantly improving its thermal resistance, oxidation resistance, and wear resistance. The findings of this research not only advance the development of HEA materials but also introduce a new technological pathway for fabricating fibre materials, offering broad application prospects and practical significance in advanced materials engineering.

**Figure 8.** Macroscopic morphology of high-entropy alloy fibers [84].

Recent studies have demonstrated that high-entropy alloy (HEA) fibers exhibit exceptional mechanical properties and high potential for extreme environment applications [83]. Compared to bulk HEAs, HEA fibers benefit from grain refinement, improved specific strength, enhanced fracture toughness, and superior high-temperature stability. The following research highlights key advancements in HEA fiber development.

Kwon et al. [85] successfully fabricated CoCrFeMnNi HEA fibers using cryogenic drawing at 77 K. The resulting fibers exhibited an exceptionally high yield strength exceeding 1500 MPa, primarily attributed to high-density dislocation accumulation and deformation twinning induced during the cryogenic drawing process. Moreover, the fibers exhibits excellent resistance to hydrogen embrittlement (HE), a property critical for structural components in hydrogen-rich environments. This superior performance is attributed to the FCC structure, which impedes hydrogen diffusion, as well as significant lattice distortion and slow diffusion effects that further suppress hydrogen penetration [83]. These findings indicate that high-strength, hydrogen-resistant HEA fibers have promising applications in fasteners and structural components for hydrogen storage and transportation systems.

Huo et al. [86] conducted a systematic study on the mechanical properties of CoCrFeNi HEA wires under both low-temperature (223 K, ~−50 °C) and high-temperature (>873 K) conditions. At low temperatures, the HEA wire exhibited an exceptionally high tensile yield strength of 1.2 GPa, while maintaining good ductility (13.6% elongation). This behavior was attributed to solid-solution strengthening, lattice distortion effects, and high dislocation density induced by the high-entropy effect, which synergistically enhanced both strength and plasticity. At high temperatures (>873 K), the HEA wire retained high strength, demonstrating excellent thermal stability.

These findings suggest that HEA wires outperform conventional alloys in extreme temperature environments, making them highly suitable for applications in aerospace structures, deep-sea equipment, and cryogenic storage systems. Additionally, this study provides critical experimental evidence for understanding the temperature dependence of HEA mechanical behavior.

Zhou et al. [87] successfully developed a biomimetic bamboo-fiber-like heterogeneous microstructure in $AlCoCrFeNi_{2.1}$ eutectic HEAs. Through multiple cold drawings and subsequent annealing, a hard $B_2$-phase fiber structure embedded in an FCC matrix was formed, mimicking the hierarchical structure of bamboo fibers. This biomimetic structure enhanced both strength and ductility, as the incompatibility between the $B_2$-phase fibers and the FCC matrix induced strain gradients, resulting in a significant heterogeneous deformation-induced (HDI) hardening effect. The HDI hardening effect increased the FCC matrix's yield strength while improving strain-hardening capacity, which delayed the localization of brittle $B_2$ fibers and improved overall tensile ductility.

It confirms that HEA fibers offer superior mechanical properties compared to traditional bulk HEAs, particularly in extreme environments. The advantages of HEA fibers include:

1. Grain Refinement & Strength Enhancement—Fibrous morphology improves specific strength and stiffness, preventing premature failure.
2. Fracture Toughness & Fatigue Resistance—High aspect ratios allow uniform stress distribution, reducing fatigue-induced damage.
3. High-Temperature Stability—HEA fibers maintain high strength and ductility even at elevated temperatures.
4. Hydrogen Embrittlement Resistance—The FCC structure and slow diffusion effects significantly suppress hydrogen penetration, making them ideal for hydrogen energy applications [88].

With these exceptional properties, HEA fibers have significant potential in aerospace, hydrogen storage systems, extreme-temperature environments, flexible electronics, and advanced fastening components. Future research should focus on scalable fabrication techniques, microstructural optimization, and multi-functional HEA fiber composites to further expand their engineering applications.

## 3. Main Fabrication Methods of High-Entropy Fibers

### *3.1. Fabrication Methods for High-Entropy Ceramic Fibers*

Electrospinning is a widely used technique for fabricating nanofibers, consisting of a spinneret, a high-voltage power supply, and a collector. The principle involves applying a high electric voltage between the spinneret and the collector, causing the polymer solution or melt to become electrically charged. When the electrostatic force overcomes the surface tension, a jet forms and undergoes rapid stretching, solvent evaporation, and solidification, ultimately depositing as nano- or micro-scale fibers on the collector [20,27,89]. Notably, combining electrospinning with post-annealing treatment often enhances the properties of the fabricated fibers.

Zhao et al. [28] first synthesized $(La_{0.2}Sm_{0.2}Eu_{0.2}Gd_{0.2}Tm_{0.2})_2Zr_2O_7$high-entropy ceramic nanofibers (HE-$RE_2Zr_2O_7$ fibers) via electrospinning. The study found that HE-$RE_2Zr_2O_7$ fibers exhibited a pure phase with uniform rare-earth element distribution and no phase segregation. Wei et al. [32] synthesized $(La_{0.25}Nd_{0.25}Sm_{0.25}Gd_{0.25})_{0.75}Yb_{0.25})_2Zr_2O_7$ ultrafine high-entropy rare-earth zirconate (HEC) fibers using sol-gel and electrospinning methods. Li et al. [29] fabricated $(La_{0.2}Nd_{0.2}Sm_{0.2}Dy_{0.2}Yb_{0.2})_2Zr_2O_7$ (HE-$RE_2Zr_2O_7$) ceramic nanofibers via electrospinning and annealing. Stanford University developed a highly efficient, low-cost, and semi-transparent air filter using electrospun polyacrylonitrile (PAN) nanofibers. These findings indicate that electrospun HEC fibers, combined with controlled calcination conditions, can be effectively tailored for high-temperature applications, sensors, and energy storage devices.

Electrospinning enables the fabrication of nanofiber-based materials with unique properties, offering novel solutions for high-performance applications. Su et al. [27] synthesized rock-salt-structured high-entropy oxide (HEO) nanofibers via electrospinning. Sun et al. [17] fabricated high-entropy $(Y_{0.2}Sm_{0.2}Gd_{0.2}Er_{0.2}Ho_{0.2})_3NbO_7$ ($5RE_3NbO_7$) nanofibers via electrospinning and calcination.The defect-fluorite structure was enhanced after calcination at 900 °C. Lü et al. [90] synthesized $(Eu_{0.2}Bi_{0.2}Y_{0.2}La_{0.2}Cr_{0.2})_2O_3$ high-entropy oxide nanofibers using electrospinning and layer-by-layer hot pressing.

These findings demonstrate the potential of high entropy materials and nanostructure design in energy storage and thermal management. Due to their multi-element composition and fibrous morphology, HEA fibers offer superior electromagnetic shielding. Their high electrical conductivity and large surface area enhance their ability to reflect and absorb electromagnetic waves, achieving high-performance broadband shielding. Zhang et al. [91] from Anhui

University fabricated honeycomb-structured porous carbon nanofiber/high-entropy alloy (HCNF/HEA) composites using electrospinning and Joule heating. FeCoNiCuMn HEA was uniformly distributed in the CNF matrix, forming a highly porous honeycomb structure. The multi-phase interface and high-entropy effect significantly enhanced electromagnetic wave absorption, making HCNF/HEA an ideal lightweight electromagnetic interference (EMI) shielding material.

This section discusses electrospinning as a key fabrication technique for high-entropy fibers, which has been widely applied in: Solid oxide fuel cells, High-temperature thermal insulation, Energy storage/Electromagnetic shielding and wave absorption. Future research will focus on structural optimization and performance enhancement to meet the demands of extreme environmental applications.

### *3.2. Fabrication Methods for High-Entropy Alloy Fibers*

The fabrication methods for high-entropy alloy (HEA) fibers primarily include rotary swaging and drawing, cryogenic rolling, and glass-cladding drawing techniques (as shown in Figure 9).

- Rotary Swaging and Drawing: This process involves hot rotary swaging followed by hot drawing, where HEA rods are processed into fiber form through repeated plastic deformation.
- Cryogenic Rolling: HEAs are subjected to rolling and extrusion at liquid nitrogen temperatures, enabling the production of fibers with precisely controlled diameters while enhancing dislocation density and mechanical strength.
- Glass-Cladding Drawing: This method utilizes glass cladding and fiber drawing techniques to fabricate micron-scale HEA fibers, ensuring uniformity and high aspect ratios.

These fabrication approaches endow HEA fibers with distinct mechanical advantages and broaden their application potential across advanced structural materials, high-temperature environments, and functional engineering applications.

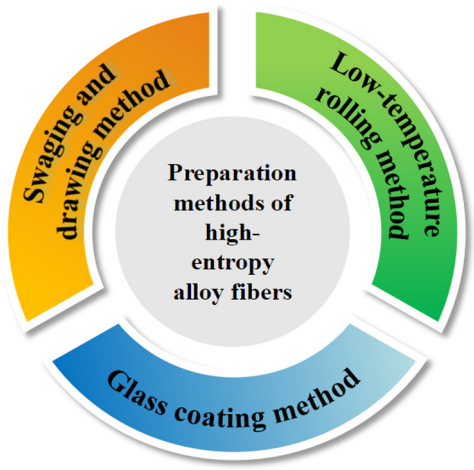


**Figure 9.** Preparation Methods of High-Entropy Alloy Fibers.

The rotary swaging and drawing process is a high-plasticity metalworking technique that integrates hot rotary swaging and hot drawing, primarily used for producing high-strength alloy wires [92,93]. During rotary swaging, the material undergoes multi-directional compressive deformation at controlled temperatures, effectively refining grain structure and optimizing texture, thereby enhancing both strength and ductility. Subsequently, the hot drawing process further reduces the wire diameter, improving uniformity and densification. This method minimizes processing defects while enhancing fatigue and corrosion resistance, making it widely applicable in high-strength cables, aerospace, and wear-resistant component manufacturing [92].

For instance, Li et al. [84] successfully fabricated high-entropy alloy (HEA) fibers with diameters ranging from 1 mm to 3.15 mm, composed of $Al_{0.3}CoCrFeNi$, using this technique. Detailed TEM analyses revealed that the enhanced mechanical properties at 77 K (*i.e.*, increased strength and ductility) were attributed to a transition in deformation mechanism from planar dislocation slip to nano-twinning. This property enhancement suggests that HEA fibers fabricated via this method may be advantageous for cryogenic applications.

Li et al. [94] further optimized the microstructure of $Al_{0.3}CoCrFeNi$ HEA fibers through an annealing process to improve their ductility. This study confirms that the rotary swaging and drawing process, by integrating hot rotary

swaging and hot drawing, can significantly refine grains, optimize texture, enhance fiber strength and ductility, and reduce defect sensitivity, thereby endowing HEA fibers with superior mechanical properties and workability.

Cryogenic Temperature Caliber Rolling (CTCR) is a severe plastic deformation technique conducted under extremely low temperatures (e.g., 77 K in liquid nitrogen) [95–97]. This method applies intensive strain through multi-pass rolling, effectively refining grain structures down to the sub-100 nm level and promoting twinning deformation, leading to a significant enhancement in both strength and ductility. The cryogenic environment suppresses dislocation recovery, thereby increasing dislocation density. Meanwhile, the FCC structure and severe lattice distortion act as barriers to hydrogen diffusion, which improves hydrogen embrittlement resistance. This technique is particularly suitable for high-strength bolts, fasteners, and other structural materials requiring both high strength and durability.

Kwon et al. [85] employed the CTCR technique to fabricate ultra-high-strength CoCrFeMnNi HEA wires with superior hydrogen embrittlement resistance. The CTCR process was performed at 77 K (liquid nitrogen temperature), where the alloy rods were continuously rolled through multiple passes, reducing their diameter from 12.5 mm to 7.5 mm, achieving a total area reduction of 64%. Before each rolling pass, the samples were immersed in liquid nitrogen to maintain the low-temperature condition, ensuring that the material experienced intense plastic deformation under cryogenic conditions. This process significantly promoted twinning deformation, leading to ultrafine grains (sub-100 nm level). Compared to conventional rolling at ambient temperature, CTCR-induced grain refinement, twinning strengthening, and dislocation accumulation resulted in a remarkable increase in tensile strength (up to 1.7 GPa) and improved resistance to hydrogen embrittlement. These findings highlight the potential of CTCR as an effective processing strategy for high-entropy alloys in high-strength bolts, fasteners, and other demanding applications.

The Taylor-Ulitovsky glass-coating method is a precision processing technique used to fabricate micro-/nano-scale high-entropy alloys [98,99]. This method involves encapsulating molten HEA with a glass layer, followed by drawing or fiberization under controlled conditions to form elongated fine fibers upon cooling. The glass encapsulation provides uniform cooling, prevents oxidation, and can be removed post-processing to obtain high-purity fibers [88]. This technique is particularly advantageous for producing ultrafine, uniform, and high-strength alloy fibers, making it widely applicable in electronic devices, precision sensors, and high-temperature wear-resistant materials.

Yan et al. [100] proposed a glass-coated high-entropy amorphous alloy fiber-reinforced aluminum matrix composite and its fabrication method. By coating the high-entropy amorphous alloy fibers with a glass layer and uniformly dispersing them within the aluminum matrix, the composite exhibits significantly enhanced interfacial bonding strength, mechanical properties, and high-temperature stability. This approach is suitable for developing high-performance structural materials in aerospace and advanced equipment applications.

This section reviewed three primary fabrication techniques for high-entropy alloy fibers: rotary swaging and drawing, cryogenic temperature caliber rolling (CTCR), and the Taylor-Ulitovsky glass-coating method [3,84–88,94]. These studies demonstrate that optimization of processing techniques enables HEA fibers to exhibit superior mechanical properties and microstructural stability, offering great potential for applications in aerospace, energy storage, and high-strength structural materials.

## 4. Challenges and Development Trends of High-Entropy Fibers

Despite the significant advantages of high-entropy fibers, their preparation processes, material design, and application development and so on still face numerous challenges. Table 1 presents the summary of representative high-entropy fibrous materials.

**Table 1.** Summary of representative high-entropy fibrous materials.

| Material System | Synthesis Method | Structure Type | Key Properties | Potential/Explored Applications |
|---|---|---|---|---|
| HEA | Melt spinning, electrospinning + reduction | Amorphous, nanocrystalline | High strength, high ductility, corrosion resistance | Aerospace fasteners, gas turbine blade coatings |
| HEO | Sol–gel electrospinning, solution spinning + sintering | Polycrystalline, nanofibrous membranes | High catalytic activity, large specific surface area, tunable bandgap | Photocatalysis/ electrocatalysis, gas sensors |
| HEC | Electrospinning + carbothermal conversion, CVD | Nanocrystalline, whiskers | Ultra-high hardness, high melting point, excellent thermal stability | Ultra-high temperature insulation, wear-resistant coatings, cutting tools |

| | | | | |
|---|---|---|---|---|
| HEN | Reactive sputtering, ALD | Nanocolumnar crystals, thin film coatings | High hardness, wear resistance, oxidation resistance | Protective coatings, surface strengthening of tools |
| HE MAX phase | Powder metallurgy/ directional solidification | Layered fibrous structures | Machinable ceramic behavior, high-temperature damage tolerance | High-temperature structural components, nuclear materials |

**Source:** Author's summary based on relevant literature including [39,40,83,101–105].

### *4.1. Complexity in Material Design and Microstructural Control*

#### 4.1.1. Risk of Phase Separation and Elemental Segregation

Due to the multi-principal element nature of high-entropy systems, phase separation and elemental segregation often occur during melt spinning or heat treatment, leading to the undesired formation of secondary phases and degradation of the designed single-phase solid solution structure. To mitigate such risks, several strategies have been proposed, including:

- precise control of cooling rates (e.g., optimized melt quenching techniques [85]);
- microalloying with elements such as B and C to suppress the formation of harmful phases;
- thermodynamic modeling (e.g., CALPHAD [106]) and phase-field simulations [107] to guide alloy design and avoid composition zones prone to phase instability.

#### 4.1.2. Challenges in Microstructural Precision

Achieving uniform and stable control of nanocrystalline, amorphous, or textured microstructures at the fiber scale (micron level) is extremely challenging. Small fluctuations in processing parameters (e.g., temperature gradient, drawing tension) during large-scale production may lead to structural inhomogeneity. Emerging solutions include the development of in-situ monitoring techniques (e.g., high-speed thermal imaging, acoustic emission) for real-time feedback control and biomimetic structural designs (e.g., core-shell architectures) to enhance the overall performance and stability of the fibers [108].

### *4.2. Bottlenecks in Fabrication and Scalability*

#### 4.2.1. Elemental Homogeneity and Composition Control

Achieving uniform mixing of multi-element precursors (e.g., in solution spinning) or homogenization of melts (e.g., in melt spinning) remains difficult, often resulting in axial and radial compositional fluctuations. Countermeasures include optimizing precursor preparation (e.g., using multi-metal complexes, electrospinning), enhancing melt stirring and homogenization, and exploring novel approaches such as gas atomization spinning based on powder metallurgy.

#### 4.2.2. High Fabrication Cost

The reliance on high-purity multi-metal raw materials, expensive and complex equipment (e.g., laser melt spinning, plasma systems), and stringent process control result in significantly higher costs compared to conventional fibrous materials. Potential cost-reduction strategies involve:

- utilizing industrial by-products or recycled metals as raw materials;
- lowering energy consumption via optimized low-temperature synthesis routes;
- developing simplified and scalable manufacturing processes suitable for mass production.

### *4.3. Insufficient Long-Term Stability Evaluation*

#### Lack of Durability Data

Current research primarily focuses on short-term performance assessments, with a limited understanding of long-term degradation behavior under complex service conditions (e.g., high-temperature oxidation/corrosion, cyclic loading, irradiation). There is an urgent need to conduct long-duration in-situ evaluations under realistic operating environments and combine these with advanced microstructural characterization (e.g., APT, TEM [109]) to elucidate the degradation mechanisms.

### *4.4. Absence of Industrial Standards*

Lack of Databases and Evaluation Criteria

The absence of systematic material databases, standardized design guidelines, and performance evaluation protocols for high-entropy fibrous materials hinders the selection, engineering applications, and commercialization of these materials. It is essential to promote collaborative efforts among academia, industry, and standardization bodies to establish shared databases and accelerate the development of relevant standards.

### *4.5. Future Development Trends Will Mainly Focus on the Following Aspects*

1. Diversification of material design: By further optimizing the composition design of high-entropy fibers and combining the demands of various fields, high-performance high-entropy fiber materials will be developed.
2. Exploration of efficient preparation processes: By integrating advanced nanotechnology and intelligent manufacturing techniques, efficient and cost-effective methods for producing high-entropy fibers will be explored.
3. Functionalization and diversified applications: The development of more applications of high-entropy fibers in fields such as smart materials, environmental protection, and biomedicine, driving technological breakthroughs and innovations across these areas.

## 5. Conclusions

### *5.1. The Microstructure and Multiscale Interface Effects of High-Entropy Fibers Grant Them Unique Properties*

The uniform distribution of multiple components and the high-entropy effect in high-entropy fiber materials contribute to their superior performance in areas such as mechanical, thermal, electrical, and chemical properties. For example, high-entropy ceramic fibers exhibit high oxidation resistance and thermal stability in high-temperature environments, making them suitable for high-temperature structural materials. On the other hand, structural variations of high-entropy alloys, such as fiber diameter, porosity and phase composition, play a critical role in determining the performance of HEA-based fibrous materials. Finer fiber diameters and uniform nanostructures contribute to enhanced mechanical flexibility and thermal shock resistance, while controlled porosity improves the specific surface area, making the fibers suitable for catalysis and filtration. Moreover, phase stability under high-temperature treatment ensures long-term functionality in extreme environments.

### *5.2. Advanced Fabrication Techniques for High-Entropy Fibers Broaden Their Application Range*

Currently, the preparation methods for high-entropy fibers include electrospinning, sol-gel methods, chemical vapor deposition (CVD), rotary-drawing, low-temperature rolling, and glass-coating methods. Among them, electrospinning combined with calcination can produce high-entropy oxide nanofibers, which are suitable for battery electrode materials and gas sensors. The glass-coating method is useful for producing high-entropy alloy micron wires, enhancing their mechanical properties and durability. These fabrication techniques have enabled the widespread application of high-entropy fibers in fields such as energy storage, flexible electronics, catalysis, environmental protection, and high-temperature protection.

### *5.3. Challenges in High-Entropy Fiber Research and Future Directions Towards Intelligent and Multifunctional Materials*

Although high-entropy fibers demonstrate vast application potential, challenges remain regarding material stability, composition optimization, control over the fabrication process, and large-scale production. Future research will focus on optimizing composition design to enhance the high-entropy effect and developing high-performance composite fiber materials. Furthermore, combining artificial intelligence in material design, nanomanufacturing techniques, and biomimetic structural designs, high-entropy fibers are expected to evolve into intelligent, adaptive, and tunable multifunctional materials, further promoting their applications in aerospace, smart materials, and new energy fields.

## Author Contributions

Conceptualization, Y.W. and X.S.; Validation, Y.W., Z.W. (Zeyu Wang) and T.D.; Investigation, Y.W.; Writing—Original Draft Preparation, Y.W.; Writing—Review & Editing, Z.Y., S.H., G.Y. and L.W.; Supervision, Z.Y., G.Y., G.Q. and Z.W. (Zhi Wang).

## Ethics Statement

Not applicable.

## Informed Consent Statement

Not applicable.

## Data Availability Statement

The data that support the findings of this study are available from the corresponding author upon reasonable request.

## Funding

This work is financially supported by the Natural Science Foundation of Hebei Province (E2021210094 and E2022210067).

## Declaration of Competing Interest

The authors declared that they have no conflicts of interest to this work. We declare that we do not have any commercial or associative interest that represents a conflict of interest in connection with the work submitted.

## References

1. Liu C, Li S, Zheng Y, Xu M, Su H, Miao X. Advances in high entropy oxides: synthesis, structure, properties and beyond. *Prog. Mater. Sci.* **2025**, *148*, 101385. doi:10.1016/j.pmatsci.2024.101385.
2. Ren J, Kumkale VY, Hou H, Kadam VS, Jagtap CV, Lokhande PE. A review of high-entropy materials with their unique applications. *Adv. Compos. Hybrid. Mater.* **2025**, *8*, 195. doi:10.1007/s42114-025-01275-4.
3. Zhou Y, Shen X, Qian T, Yan C, Lu J. A review on the rational design and fabrication of nanosized high-entropy materials. *Nano Res.* **2023**, *16*, 7874–7905. doi:10.1007/s12274-023-5419-2.
4. Liu J, Li Z, Lin D, Tang Z, Song X, He P. Eutectic high-entropy alloys and their applications in materials processing engineering: A review. *J. Mater. Sci. Technol.* **2024**, *189*, 211–246. doi:10.1016/j.jmst.2023.10.057.
5. Ma B, Fan D, Zhang G, Liao Y, Shen Z, Lu Y. Configurations Manipulation of Electrospun Membranes Based on High-Entropy Alloys–Enabled High-Performance Solar Water Evaporation. *Sol. RRL* **2023**, *7*, 2300484. doi:10.1002/solr.202300484.
6. Andrade G, Zepon G, Edalati K, Mohammadi A, Ma Z, Li H.-W, et al. Crystal structure and hydrogen storage properties of AB-type TiZrNbCrFeNi high-entropy alloy. *Int. J. Hydrogen Energy* **2023**, *48*, 13555–13565. doi:10.1016/j.ijhydene.2022.12.134.
7. Li J, Fan H, Zhang Q, Chen H, Su Y, Song J, et al. Carbon vacancies enhanced oxidation resistance of high-entropy carbides $(Ti_{0.2}V_{0.2}Nb_{0.2}Mo_{0.2}W_{0.2})C$. *Ceram. Int.* **2024***, 50*, 9926–9930. doi:10.1016/j.ceramint.2023.12.311.
8. Lou BS, Li CL, Annalakshmi M, Hung TY, Lee JW. Exploring the effect of Ti and Al contents on the microstructural, mechanical, and corrosion resistance features of VNbMoTaWTiAlN refractory high entropy alloy coatings. *Mater. Chem. Phys.* **2025**, *341*, 130901. doi:10.1016/j.matchemphys.2025.130901.
9. Shen H, Zhang J, Hu J, Zhang J, Mao Y, Xiao H, et al. A Novel TiZrHfMoNb High-Entropy Alloy for Solar Thermal Energy Storage. *Nanomaterials* **2019**, *9*, 248. doi:10.3390/nano9020248.
10. Guo W, Hu J, Fang W, Ye Y, Zhang S, Bai S. A novel strategy for rapid fabrication of continuous carbon fiber reinforced (TiZrHfNbTa)C high-entropy ceramic composites: High-entropy alloy in-situ reactive melt infiltration. *J. Eur. Ceram. Soc.* **2023**, *43*, 2295–2305. doi:10.1016/j.jeurceramsoc.2023.01.019.
11. Yuan M, Gao Y, Liu L, Gao J, Wang Z, Li Y, et al. High entropy double perovskite cathodes with enhanced activity and operational stability for solid oxide fuel cells. *J. Eur. Ceram. Soc.* **2024**, *44*, 3267–3276. doi:10.1016/j.jeurceramsoc.2023.12.049.
12. Wang Y, Mi J, Wu ZS. Recent status and challenging perspective of high entropy oxides for chemical catalysis. *Chem. Catal.* **2022**, *2*, 1624–1656. doi:10.1016/j.checat.2022.05.003.
13. Hirai T, Yagi K, Nakai K, Okamoto K, Murai D, Okamoto H. High-entropy polymer blends utilizing in situ exchange reaction. *Polymer* **2022**, *240*, 124483. doi:10.1016/j.polymer.2021.124483.
14. Lashkari AH, Ostovari Moghaddam A, Naseri M, Shokuhfar A. Synthesis and characterization of high entropy carbide-MAX two-phase composites. *J. Mater. Res. Technol.* **2023**, *24*, 5024–5031. doi:10.1016/j.jmrt.2023.04.125.
15. Wei Z, Mei D, Wei Z, Cheng J, Lin J, Hong S. Thick $(AlTiCrNbTa)O_2$ high-entropy ceramic coating: Efficient fabrication and characterization. *Ceram. Int.* **2024**, *50*, 33085–33092. doi:10.1016/j.ceramint.2024.06.042.

16. Deng Q, Xue L, Ma M, Du J, Xin H, Chen H, et al. A novel high-entropy $(Y_{0.2}La_{0.2}Er_{0.2}Ho_{0.2}Tm_{0.2})_6MoO_{12}$ ceramic nanofibers with high near-infrared reflection and low thermal conductivity. *J. Eur. Ceram. Soc.* **2025**, *45*, 117461. doi:10.1016/j.jeurceramsoc.2025.117461.
17. Sun X, Sun G, Huang M. Novel high entropy $(Y_{0.2}Sm_{0.2}Gd_{0.2}Er_{0.2}Ho_{0.2})_3NbO_7$ nanofibers with ultralow thermal conductivity. *J. Am. Ceram. Soc.* **2024**, *107*, 1408–1418. doi:10.1111/jace.19533.
18. Du X, Zhang K. Recent progress in fibrous high-entropy energy harvesting devices for wearable applications. *Nano Energy* **2022**, *101*, 107600. doi:10.1016/j.nanoen.2022.107600.
19. Zhu S, Shi S, Xie Y, Xu C, Zhang X, Peng Y, et al. Electrospinning $SnO_2$ fibers with 3D interconnected structure for efficient soot catalytic combustion. *J. Mater. Sci.* **2020**, *55*, 16083–16095. doi:10.1007/s10853-020-05198-x.
20. Wang Q, Ji S, Li S, Zhou X, Yin J, Liu P, et al. Electrospinning visible light response Bi2MoO6/$Ag_3PO_4$ composite photocatalytic nanofibers with enhanced photocatalytic and antibacterial activity. *Appl. Surf. Sci.* **2021**, *569*, 150955. doi:10.1016/j.apsusc.2021.150955.
21. Song Z, Yu S, Wang K, Jiang Z, Xue L, Yang F. Novel Sc-doped Bi3TiNbO9 ferroelectric nanofibers prepared by electrospinning for visible-light photocatalysis. *J. Rare Earths* **2023**, *41*, 365–373. doi:10.1016/j.jre.2022.01.010.
22. Bib Khan J, Kumar Panda P, Dash P, Hsieh C. Microwave-Assisted Synthesis of Platinum-free High-Entropy Alloy Catalysts on Reduced Graphene Oxide Sheets for Enhanced Oxygen Reduction and Evolution Reactions. *Chem—Eur. J.* **2025**, *31*, e202403863. doi:10.1002/chem.202403863.
23. Gu S, Huang H.-Y, Lin Y.-C, Hsieh C.-A, Panda P. K, et al. High-entropy alloys with low platinum content: novel catalysts for oxygen reduction and evolution reactions. *Emergent Mater.* **2025**, *6*, 1–14 doi:10.1007/s42247-025-01011-0.
24. Panda PK, Huang HY, Dash P, Hsieh CT, Chang JK, Liu WR. Liquid-phase microwave synthesis of platinum-based high-entropy alloy catalysts on carbon supports for electrochemical hydrogen adsorption/desorption and oxygen evolution/reduction reactions. *Int. J. Hydrogen Energy* **2025**, *111*, 536–545. doi:10.1016/j.ijhydene.2025.02.312.
25. Chen H, Jie K, Jafta C. J, Yang Z, Yao S, Liu M, et al. An ultrastable heterostructured oxide catalyst based on high-entropy materials: A new strategy toward catalyst stabilization via synergistic interfacial interaction. *Appl. Catal. B Environ.* **2020**, *276*, 119155. doi:10.1016/j.apcatb.2020.119155.
26. Liu S, Du M, Ge Y, Li Z, Srivastava G. P, Wang J, et al. Enhancement of high entropy oxide $(La_{0.2}Nd_{0.2}Sm_{0.2}Gd_{0.2}Y_{0.2})_2Zr_2O_7$ mechanical and photocatalytic properties via Eu doping. *J. Mater. Sci.* **2022**, *57*, 7863–7876. doi:10.1007/s10853-022-07124-9.
27. Su J, Cao Z, Jiang Z, Chen G, Zhu Y, Wang L, et al. High entropy oxide nanofiber by electrospun method and its application for lithium battery anode material. *Int. J. Appl. Ceram. Technol.* **2022**, *19*, 2004–2015. doi:10.1111/ijac.14021.
28. Zhao W, Yang F, Liu Z, Chen H, Shao Z, Zhang X, et al. A novel $(La_{0.2}Sm_{0.2}Eu_{0.2}Gd_{0.2}Tm_{0.2})_2Zr_2O_7$ high-entropy ceramic nanofiber with excellent thermal stability. *Ceram. Int.* **2021**, *47*, 29379–29385. doi:10.1016/j.ceramint.2021.07.105.
29. Li Z, Zhou F, Xu B, Guo D. Characterization of novel high-entropy $(La_{0.2}Nd_{0.2}Sm_{0.2}Dy_{0.2}Yb_{0.2})_2Zr_2O_7$ electrospun ceramic nanofibers. *Ceram. Int.* **2022**, *48*, 12074–12078. doi:10.1016/j.ceramint.2022.01.067.
30. Xing Y, Dan W, Fan Y, Li X. Low temperature synthesis of high-entropy $(Y_{0.2}Yb_{0.2}Sm_{0.2}Eu_{0.2}Er_{0.2})_2O_3$ nanofibers by a novel electrospinning method. *J. Mater. Sci. Technol.* **2022**, *103*, 215–220. doi:10.1016/j.jmst.2021.06.057.
31. Li W, Sun Y, Ye L, Han W, Chen F, Zhang J, et al. Preparation of high entropy nitride ceramic nanofibers from liquid precursor for $CO_2$ photocatalytic reduction. *J. Am. Ceram. Soc.* **2022**, *105*, 3729–3734. doi:10.1111/jace.18384.
32. Wei M, Xu J, Yang R, Zhu J, Meng X, Yang J, et al. Synthesis of ultra-fine rare-earth-zirconate high-entropy ceramic fibers via electrospinning. *J. Am. Ceram. Soc.* **2022**, *105*, 4449–4456. doi:10.1111/jace.18415.
33. El-Kholy R. A, Isawi H, Zaghlool E, Soliman E. A, Khalil M. M. H, Said M. M, et al. Preparation and characterization of rare earth element nanoparticles for enhanced photocatalytic degradation. *Environ. Sci. Pollut. Res.* **2023**, *30*, 69514–69532. doi:10.1007/s11356-023-27090-2.
34. Štamborská M, Pelachová T, Danko D, Orovčík L. Influence of hot forging on grain formation in Al0.35CoCrFeNi high-entropy alloy: numerical simulation, microstructure and mechanical properties. *Arch. Civ. Mech. Eng.* **2024**, *24*, 241. doi:10.1007/s43452-024-01051-z.
35. Wan Y, Wei W, Ding S, Wu L, Qin H, Yuan X. A Multi-Site Synergistic Effect in High-Entropy Alloy for Efficient Hydrogen Evolution. *Adv. Funct. Mater.* **2025**, *35*, 2414554. doi:10.1002/adfm.202414554.
36. Shao Y, Xu J, Wei M, Wang H, Lin L, Fan F, et al. Rare-earth zirconate high-entropy nanofibrous porous ceramics for high-temperature thermal insulation applications. *J. Eur. Ceram. Soc.* **2023**, *43*, 7635–7643. doi:10.1016/j.jeurceramsoc.2023.08.016.
37. Wen Y, Liu Y. Quantitative analysis of atomic-scale local lattice distortions in high-entropy fluorite oxide $(Zr_{0.2}Ce_{0.2}Hf_{0.2}Y_{0.2}Al_{0.2})O_2$-δ. *Ceram Int.* **2023**, *49*, 26141–26146.
38. Chen H, Fu J, Zhang P, Peng H, Abney C. W, Jie K, et al. Entropy-stabilized metal oxide solid solutions as CO oxidation catalysts with high-temperature stability. *J. Mater. Chem. A* **2018**, *6*, 11129–11133. doi:10.1039/C8TA01772G.
39. Oses C, Toher C, Curtarolo S. High-entropy ceramics. *Nat. Rev. Mater.* **2020**, *5*, 295–309. doi:10.1038/s41578-019-0170-8.

40. Akrami S, Edalati P, Fuji M, Edalati K. High-entropy ceramics: Review of principles, production and applications. *Mater. Sci. Eng. R. Rep.* **2021**, *146*, 100644. doi:10.1016/j.mser.2021.100644.
41. Spiridigliozzi L, Ferone C, Cioffi R, Dell'Agli G. A simple and effective predictor to design novel fluorite-structured High Entropy Oxides (HEOs). *Acta Mater.* **2021**, *202*, 181–189. doi:10.1016/j.actamat.2020.10.061.
42. Zhao Z, Chen H, Xiang H, Dai F.-Z, Wang X, Xu W, et al. High entropy defective fluorite structured rare-earth niobates and tantalates for thermal barrier applications. *J. Adv. Ceram.* **2020**, *9*, 303–311. doi:10.1007/s40145-020-0368-7.
43. Ma B, Wen Z, Qin J, Wu Z, Liu J, Lv Y, et al. Synthesis and microstructure of $(Ce_{0.2}Zr_{0.2}La_{0.2}Sm_{0.2}Nd_{0.2})O_2$-δ high-entropy oxides characterized by fluorite structure. *Ceram. Int.* **2024**, *50*, 1981–1989. doi:10.1016/j.ceramint.2023.10.303.
44. Chen Y, Zhou S, Li J, Li S, Zhao H, Zhang M, et al. Influence of synergistic effect on the structure and dielectric property of $La_2(TiZrSnHfGe)_2O_7$ high entropy oxides. *Ceram. Int.* **2024**, *50*, 39493–39503. doi:10.1016/j.ceramint.2024.07.327.
45. Li Z, Li J, Zhao H, Zhang M, Li P, Dong L, et al. Influence of atmosphere-induction and synergistic effect on the dielectric property of rutile-type $(Ge_{0.2}Mn_{0.2}Ti_{0.2}Sn_{0.2}Mo_{0.2})O_2$ high-entropy oxides. *J. Alloys Compd.* **2024**, *1002*, 175246. doi:10.1016/j.jallcom.2024.175246.
46. Liu Z, Wei C, De Y, Zhang S, Zhang C, Li X. Phase structure of high-entropy pyrochlore oxides: From powder synthesis to ceramic sintering. *J. Eur. Ceram. Soc.* **2023**, *43*, 7613–7622. doi:10.1016/j.jeurceramsoc.2023.08.008.
47. Zhou S, Pu Y, Zhang Q, Shi R, Guo X, Wang W, et al. Microstructure and dielectric properties of high entropy $Ba(Zr_{0.2}Ti_{0.2}Sn_{0.2}Hf_{0.2}Me_{0.2})O_3$ perovskite oxides. *Ceram. Int.* **2020**, *46*, 7430–7437. doi:10.1016/j.ceramint.2019.11.239.
48. Yan S, Sun X, Wang G, Zhang L, Li H, Li H. Preparation Method of High Entropy Oxide Ceramic Fiber Material. CN113754432A, 30 September 2021.
49. Liew S. L, Zhou J, Wei F, Ni X. P, Tan S. Y, Lim P. C, et al. Design and synthesis of single phase $Hf_{0.25}Zr_{0.25}Ce_{0.25}Y_{0.125}Si_{0.125}O_2$-δ high-entropy ceramics. *J. Alloys Compd.* **2022**, *904*, 164097. doi:10.1016/j.jallcom.2022.164097.
50. Wen Y, Liu Y. Processing and microstructure of a fluorite high-entropy oxide $(Zr_{0.2}Ce_{0.2}Hf_{0.2}Y_{0.2}Al_{0.2})O_2$-δ. *Ceram. Int.* **2022**, *48*, 2546–2554. doi:10.1016/j.ceramint.2021.10.037.
51. Ye F, Meng F, Luo T, Qi H. Ultrafast high-temperature sintering of high-entropy $(La_{0.2}Nd_{0.2}Sm_{0.2}Eu_{0.2}Gd_{0.2})_2Hf_2O_7$ ceramics with fluorite structure. *Ceram. Int.* **2022**, *48*, 35649–35654. doi:10.1016/j.ceramint.2022.09.041.
52. Ozlu Torun H, Çakar S. Thermal characterization of Er-doped and Er–Gd co-doped ceria-based electrolyte materials for SOFC. *J. Therm. Anal. Calorim.* **2018**, *133*, 1233–1239. doi:10.1007/s10973-018-7189-8.
53. Akbar M, Qu G, Yang W, Gao J, Yousaf M, Mushtaq N, et al. Fast ionic conduction and rectification effect of $NaCo_{0.5}Fe_{0.5}O_2$-$CeO_2$ nanoscale heterostructure for LT-SOFC electrolyte application. *J. Alloys Compd.* **2022**, *924*, 166565. doi:10.1016/j.jallcom.2022.166565.
54. Zhang J, Liang J, Li H, Yang Y, Huo D, Liu C. A review of high-entropy ceramics preparation methods, properties in different application fields and their regulation methods. *J. Mater. Res. Technol.* **2024**, *32*, 1083–1117. doi:10.1016/j.jmrt.2024.07.153.
55. Liu J, Li Y, Chen Z, Liu N, Zheng L, Shi W, et al. Polyoxometalate Cluster-Incorporated High Entropy Oxide Sub-1 nm Nanowires. *J. Am. Chem. Soc.* **2022**, *144*, 23191–23197. doi:10.1021/jacs.2c10602.
56. Deng Z, Peng Y, Qin W. W, Liu B, Zhang G, Wang X, et al. Flexible, high strength and low thermal conductivity of a novel high entropy oxide ceramic fiber membranes. *Chem. Eng. J.* **2023**, *475*, 146260. doi:10.1016/j.cej.2023.146260.
57. Zhang J, Tian J, Xing B, Wang J, Liu B, Nian H, et al. Preparation and thermal/dielectric properties of medium/high entropy perovskite titanate ceramics. *Ceram. Int.* **2024**, *50*, 29954–29965. doi:10.1016/j.ceramint.2024.05.291.
58. Shi Z, Zhang J, Wei J, Hou X, Cao S, Tong S, et al. A-site deficiency improved the thermoelectric performance of high-entropy perovskite manganite-based ceramics. *J. Mater. Chem. C* **2022**, *10*, 15582–15592. doi:10.1039/D2TC02952A.
59. Dong S.-T, Ye X, Fu Z, Jin X, Wei J, Wang L, et al. Effects of strontium substitution for La on the electrochemical performance of $LaAlO_3$ perovskite nanotubes. *J. Mater. Res. Technol.* **2022**, *19*, 91–100. doi:10.1016/j.jmrt.2022.04.150.
60. Liu Y, Hou J, Cheng C, Cheng F, Su T, Miao Y, et al. The effect of non-equimolar doping on the preparation and electrical conductivity of $Sr(Ti,Zr,Zn,Sn,Hf)O_3$-σ high entropy perovskite oxide. *Ceram. Int.* **2023**, *49*, 21546–21554. doi:10.1016/j.ceramint.2023.03.290.
61. Rizwan M, Gul S, Iqbal T, Mushtaq U, Farooq M. H, Farman M, et al. A review on perovskite lanthanum aluminate ($LaAlO_3$), its properties and applications. *Mater. Res. Express* **2019**, *6*, 112001. doi:10.1088/2053-1591/ab4629.
62. Zhang X, Liu X, Yan J, Gu Y, Qi X. Preparation and Property of High Entropy $(La_{0.2}Li_{0.2}Ba_{0.2}Sr_{0.2}Ca_{0.2})TiO_3$ Perovskite Ceramics. *J. Inorg. Mater.* **2021**, *36*, 379. doi:10.15541/jim20200500.
63. Ma C, Su T, Li Z, Ren B, Meng Z, Li B, et al. Preparation of $(Ba_{0.25}Ca_{0.25}Sr_{0.25}La_{0.25})Ti_{1-x}Al_xO_3$ high-entropy perovskite ceramics for enhanced microwave dielectric performance. *J. Alloys Compd.* **2025**, *1010*, 177719. doi:10.1016/j.jallcom.2024.177719.
64. Tian L, Zhang Z, Liu S, Li G, Gao X. High-entropy perovskite oxide nanofibers as efficient bidirectional electrocatalyst of liquid-solid conversion processes in lithium-sulfur batteries. *Nano Energy* **2023**, *106*, 108037. doi:10.1016/j.nanoen.2022.108037.

65. Fu X, Lü S, Meng X, Sun C, Wei M, Jiang H, et al. High-entropy cobalt-free perovskite as a high-performing nanofiber cathode for solid oxide fuel cells. *J. Mater. Chem. A* **2024**, *12*, 27452–27463. doi:10.1039/D4TA01803F.
66. Liu T, Chu K, Lai F. $ABO_3$-Type High-Entropy Perovskite $Bax(FeCoNiZrY)_{0.2}O_{3-\delta}$ Electrocatalytic Material and Its Preparation Method. CN113737214A, 3 December 2021.
67. Hao J, Ma F, Chen Y, Lu S, Duan F, Du M, et al. Cocktail effect in high-entropy perovskite oxide for boosting alkaline oxygen evolution. *New J. Chem.* **2024**, *48*, 511–514. doi:10.1039/D3NJ04481E.
68. Triolo C, Moulaee K, Ponti A, Pagot G, Di Noto V, Pinna N, et al. Spinel-Structured High-Entropy Oxide Nanofibers as Electrocatalysts for Oxygen Evolution in Alkaline Solution: Effect of Metal Combination and Calcination Temperature. *Adv. Funct. Mater.* **2024**, *34*, 2306375. doi:10.1002/adfm.202306375.
69. Dąbrowa J, Stygar M, Mikuła A, Knapik A, Mroczka K, Tejchman W, et al. Synthesis and microstructure of the $(Co,Cr,Fe,Mn,Ni)_3O_4$ high entropy oxide characterized by spinel structure. *Mater. Lett.* **2018**, *216*, 32–36. doi:10.1016/j.matlet.2017.12.148.
70. Grzesik Z, Smoła G, Miszczak M, Stygar M, Dąbrowa J, Zajusz M, et al. Defect structure and transport properties of $(Co,Cr,Fe,Mn,Ni)_3O_4$ spinel-structured high entropy oxide. *J. Eur. Ceram. Soc.* **2020**, *40*, 835–839. doi:10.1016/j.jeurceramsoc.2019.10.026.
71. Krysko E, Min L, Wang Y, Zhang N, Barber J. P, Niculescu G. E, et al. Studies on the structure and the magnetic properties of high-entropy spinel oxide $(MgMnFeCoNi)Al_2O_4$. *APL Mater.* **2023**, *11*, 101123. doi:10.1063/5.0161401.
72. Shi Z, Zhang X, Zheng Z, Feng X, Fang Z, Tang B. Phase compositions, microstructures, and microwave dielectric properties of novel high-entropy spinel-structured $MAl_2O_4$ ceramics. *J. Alloys Compd.* **2024**, *1004*, 175714. doi:10.1016/j.jallcom.2024.175714.
73. Zhang L, Xia S, Zhang X, Yao Y, Zhang Y, Chen S, et al. Low-Temperature Synthesis of Mesoporous Half-Metallic High-Entropy Spinel Oxide Nanofibers for Photocatalytic CO2 Reduction. *ACS Nano* **2024**, *18*, 5322–5334. doi:10.1021/acsnano.3c09559.
74. Zheng Y, Wu X, Lan X, Hu R. A Spinel $(FeNiCrMnMgAl)_3O_4$ High Entropy Oxide as a Cycling Stable Anode Material for Li-Ion Batteries. *Processes* **2021**, *10*, 49. doi:10.3390/pr10010049.
75. Li X, Chang X, Liu X, Zhang J. High-entropy oxide $(FeCoNiCrMn)_3O_4$ for room-temperature NO2 sensors. *Appl. Phys. Lett.* **2024**, *124*, 221901. doi:10.1063/5.0191206.
76. Jia H, Li C, Chen G, Gong B, Li S, Zhou Y, et al. Design, synthesis, and influencing factors of medium-/high-entropy $Y_2(ZrTiGeHfSnSi)_2O_7$ with a pyrochlore structure. *J. Eur. Ceram. Soc.* **2024**, *44*, 3296–3306. doi:10.1016/j.jeurceramsoc.2023.12.027.
77. Talanov MV, Talanov VM. Structural Diversity of Ordered Pyrochlores. *Chem. Mater.* **2021**, *33*, 2706–2725. doi:10.1021/acs.chemmater.0c04864.
78. Teng Z, Zhu L, Tan Y, Zeng S, Xia Y, Wang Y, et al. Synthesis and structures of high-entropy pyrochlore oxides. *J. Eur. Ceram. Soc.* **2020**, *40*, 1639–1643. doi:10.1016/j.jeurceramsoc.2019.12.008.
79. Wang H, Xu J, Wei M, Feng X, Wu J, Zhang P, et al. Flexible dual-phase rare-earth zirconate high-entropy ceramic nanofibrous membranes for superior thermal insulation. *J. Am. Ceram. Soc.* **2024**, *107*, 3857–3867. doi:10.1111/jace.19666.
80. Ai L, Wang Z, Gao Y, Cui C, Wang B, Liu W, et al. Effect of surface and bulk palladium doping on the catalytic activity of $La_2Sn_2O_7$ pyrochlore oxides for diesel soot oxidation. *J. Mater. Sci.* **2019**, *54*, 4495–4510. doi:10.1007/s10853-018-3160-0.
81. Dou L, Yang B, Lan S, Liu Y, Liu Y, Nan C, et al. High-Entropy-Nanofibers Enhanced Polymer Nanocomposites for High-Performance Energy Storage. *Adv. Energy Mater.* **2023**, *13*, 2203925. doi:10.1002/aenm.202203925.
82. Tsai MH, Yeh JW. High-Entropy Alloys: A Critical Review. *Mater. Res. Lett.* **2014**, *2*, 107–123. doi:10.1080/21663831.2014.912690.
83. Zhang W-T, Wang X-Q, Zhang F-Q, Cui X-Y, Fan B.-B, Guo J.-M, et al. Frontiers in high entropy alloys and high entropy functional materials. *Rare Met.* **2024**, *43*, 4639–4776. doi:10.1007/s12598-024-02852-0.
84. Li D, Li C, Feng T, Zhang Y, Sha G, Lewandowski JJ, et al. High-entropy Al0.3CoCrFeNi alloy fibers with high tensile strength and ductility at ambient and cryogenic temperatures. *Acta Mater.* **2017**, *123*, 285–294. doi:10.1016/j.actamat.2016.10.038.
85. Kwon YJ, Won JW, Park SH, Lee JH, Lim KR, Na YS, et al. Ultrahigh-strength CoCrFeMnNi high-entropy alloy wire rod with excellent resistance to hydrogen embrittlement. *Mater. Sci. Eng. A* **2018**, *732*, 105–111. doi:10.1016/j.msea.2018.06.086.
86. Huo W, Fang F, Zhou H, Xie Z, Shang J, Jiang J. Remarkable strength of CoCrFeNi high-entropy alloy wires at cryogenic and elevated temperatures. *Scr. Mater.* **2017**, *141*, 125–128. doi:10.1016/j.scriptamat.2017.08.006.
87. Zhou S, Dai C, Hou H, Lu Y, Liaw PK, Zhang Y. A remarkable toughening high-entropy-alloy wire with a bionic bamboo fiber heterogeneous structure. *Scr. Mater.* **2023**, *226*, 115234. doi:10.1016/j.scriptamat.2022.115234.
88. Chen J-X, Chen Y, Liu J-P, Liu T-W, Dai L-H. Anomalous Size Effect in Micron-Scale CoCrNi Medium-Entropy Alloy *Wire. Scr. Mater*. **2021**, *199*, 113897. https://doi.org/10.1016/j.scriptamat.2021.113897.
89. Wang J, Wang Z, Ni J, Li L. Electrospinning for flexible sodium-ion batteries. *Energy Storage Mater.* **2022**, *45*, 704–719. doi:10.1016/j.ensm.2021.12.022.

90. Jing L, Li W, Gao C, Li M, Fei W. Enhanced Energy Storage Performance Achieved in Multilayered PVDF–PMMA Nanocomposites Incorporated with High-Entropy Oxide Nanofibers. *ACS Appl. Energy Mater.* **2023**, *6*, 3093–3101. doi:10.1021/acsaem.3c00054.
91. Wang S, Liu Q, Li S, Huang F, Zhang H. Joule-Heating-Driven Synthesis of a Honeycomb-Like Porous Carbon Nanofiber/High Entropy Alloy Composite as an Ultralightweight Electromagnetic Wave Absorber. *ACS Nano* **2024**, *18*, 5040–5050. doi:10.1021/acsnano.3c11408.
92. Shi M, Liao H, Zhou J, Li G, Cui Z, Yan T, et al. Effect of High-Temperature Annealing on Microstructure and Mechanical Properties of Extremely Deformed Fe35Ni35Cr20Mn10 High-Entropy Alloy Wire. *J. Mater. Eng. Perform.* **2025**, *34*, 885–895. doi:10.1007/s11665-023-09061-3.
93. Chen JX, Li T, Chen Y, Cao FH, Wang HY, Dai LH. Ultra-strong heavy-drawn eutectic high entropy alloy wire. *Acta Mater.* **2023**, *243*, 118515. doi:10.1016/j.actamat.2022.118515.
94. Li D, Gao MC, Hawk JA, Zhang Y. Annealing effect for the Al0.3CoCrFeNi high-entropy alloy fibers. *J. Alloys Compd.* **2019**, *778*, 23–29. doi:10.1016/j.jallcom.2018.11.116.
95. Chen D, Li D, Peng J, Wang T, Yan B, Lu W. The Effect of Rolling Temperature on the Microstructure and Mechanical Properties of Surface-Densified Powder Metallurgy Fe-Based Gears Prepared by the Surface Rolling Process. *Metals* **2017**, *7*, 420. doi:10.3390/met7100420.
96. Kumar V, Kumar D. Investigation of tensile behaviour of cryorolled and room temperature rolled 6082 Al alloy. *Mater Sci Eng A* **2017**, *691*, 211–217. doi:10.1016/j.msea.2017.03.051.
97. Wu Y, Liu S, Luo K, Kong C, Yu H. Deformation mechanism and mechanical properties of a CoCrFeNi high-entropy alloy via room-temperature rolling, cryorolling, and asymmetric cryorolling. *J. Alloys Compd.* **2023**, *960*, 170883. doi:10.1016/j.jallcom.2023.170883.
98. Farag MM, Ahmed HY, Al-Rashidy ZM. Improving the Corrosion Resistance of Magnesium Alloy by Magnesium Phosphate/Glass Composite Coatings Using Sol–Gel Method. *Silicon* **2023**, *15*, 3841–3854. doi:10.1007/s12633-022-02226-0.
99. Jeong SJ, Kim MS, Kim IS, Joo HK, Lee DS. Preparation and properties of borosilicate glass-coated Cu powder for internal electrode of multilayer ceramic device. *J. Electroceram.* **2011**, *26*, 162–169. doi:10.1007/s10832-011-9640-0.
100. Yan H, Cao S, Wang J. Glass-Coated High-Entropy Amorphous Alloy Fiber Reinforced Aluminum Matrix Composite and Its Preparation Method. CN 119876796 A, 25 April 2025.
101. Tran TTT, Trinh VH, Seo J. Two-dimensional perovskite SrNbO2N with Zr doping for accelerating photoelectrochemical water splitting. *J. Mater. Sci. Technol.* **2023**, *142*, 176–184. doi:10.1016/j.jmst.2022.09.034.
102. Chen J, Liu W, Liu J, Zhang X, Yuan M, Zhao Y, et al. Stability and Compressibility of Cation-Doped High-Entropy Oxide MgCoNiCuZnO5. *J. Phys. Chem. C* **2019**, *123*, 17735–17744. doi:10.1021/acs.jpcc.9b04992.
103. Lu D, Wang C, Wang C, Tian W, Qiu S, Su GH. Numerical simulation of corrosion phenomena in oxygen-controlled environment for a horizontal lead-bismuth reactor core. *J. Nucl. Mater.* **2023**, *574*, 154195. doi:10.1016/j.jnucmat.2022.154195.
104. Popescu A-M J, Branzoi F, Constantin I, Anastasescu M, Burada M, Mitrică D, et al. Electrodeposition, Characterization, and Corrosion Behavior of CoCrFeMnNi High-Entropy Alloy Thin Films. *Coatings* **2021**, *11*, 1367. doi:10.3390/coatings11111367.
105. Sun Z, He B, Li K, Tu Y, Wang H. Study on microstructure evolution and aging precipitation behavior of a novel Al-Li alloy fabricated by laser rapid melting. *J. Alloys Compd.* **2022**, *908*, 164630. doi:10.1016/j.jallcom.2022.164630.
106. Asadikiya M, Zhang Y, Wang L, Apelian D, Zhong Y. Design of ternary high-entropy aluminum alloys (HEAls). *J. Alloys Compd.* **2022**, *891*, 161836. doi:10.1016/j.jallcom.2021.161836.
107. Wang K.-L, Yang W.-K, Shi X.-C, Hou H, Zhao Y.-H. Phase-field-method-studied mechanism of Cu-rich phase precipitation in AlxCuMnNiFe high-entropy alloy. *Acta Phys. Sin.* **2023**, *72*, 076102. doi:10.7498/aps.72.20222439.
108. Zhang Y, Fu Q, Song B, Xu P. Regulation Strategy of Transition Metal Oxide-Based Electrocatalysts for Enhanced Oxygen Evolution Reaction. *Acc. Mater. Res.* **2022**, *3*, 1088–1100. doi:10.1021/accountsmr.2c00161.
109. Liu X, Su Q, Zhu J, Song X. The Aging Behavior and Life Prediction of CFRP Rods under a Hygrothermal Environment. *Polymers* **2023**, *15*, 2490. doi:10.3390/polym15112490.